# Characterization of FePt-based Nanocomposite Thin Films Prepared by Pulsed Filtered Vacuum Arc Deposition

By

Lai Yiu Wai

Supervisor: Prof. S. P. Wong

A Thesis Submitted in Partial Fulfillment of the Requirements

for the Degree of Master of Philosophy

in

Electronic Engineering



July, 2005

# Abstract

Materials with high uniaxial magnetocrystalline anisotropy, such as FePt in fct phase, are attractive for ultra-high-density magnetic recording applications because they could provide smaller magnetic grains while maintaining a sufficiently high thermal stability.

In this work, we have prepared FePt-C and FePt-Cu multilayer films with different composition and film thickness by pulsed filtered vacuum arc deposition. Several characterization techniques were employed in this project. These include Rutherford backscattering spectrometry (RBS) for film composition determination, x-ray diffraction (XRD) to study the structure, vibrating sample magnetometery (VSM) to measure the magnetic properties, and transmission electron microscopy (TEM) for high resolution structural analysis.

FePt-C and FePt-Cu films with different thickness have been investigated for their magnetic and structural properties. Results of both series of samples show that the degree of fct phase ordering decreases with decreasing film thickness. The reduction in coercivity and grain size in thinner film supports the argument that the disorder-order transformation is grain size dependent. Grain growth limitation is achieved by reducing film thickness, but higher ordering temperature becomes the trade-off.

Moreover, C ion-implantation has been employed after multilayer film deposition. The implanted FePt-C samples were found to have similar coercivity but smaller grain size when compared with the un-implanted one. The XRD peaks ratio suggests there

is long range order in implanted sample, this explains why they have such large coercivity despite of the small grain size.

Furthermore, by changing the C/Cu spacer thickness between FePt layers, films with different composition have been investigated. It is shown that the chemical ordering of FePt greatly depends on the additive spacer thickness. The degree of fcc-fct phase transformation simply decreases with increasing spacer thickness in FePt-C samples. While in FePt-Cu films, the chemical order reaches maximum when thin Cu spacer layers are inserted between FePt layers. This indicates the phase transformation enhancement mechanisms of the two additives are different.

# 摘要

基於其在可以產生更小的磁性晶粒的同時能保持足夠高的熱穩定性的特性，單軸各向異性的磁性材料，比如 fct 相的 FePt，在高密度磁記錄領域有很大的潛在應用。

本論文利用脈衝磁過濾真空弧方法製備不同組分和厚度的 FePtC 和 FePtCu 複合磁性薄膜。使用盧瑟福背散射(NRBS)技術測定薄膜的成分，用 X-射線衍射(XRD)分析其晶體結構，用振動樣品磁強計(VSM)表徵其磁學性能，又利用透射電子顯微鏡(TEM)得出其原子結構圖像。

我們檢測了不同厚度的 FePtC 和 FePtCu 薄膜的磁學性能及結構。結果顯示 FePt 的 fct 相變程度隨著薄膜厚度減少而遞減。矯頑力值和晶粒體積的同時減小證明了有序化過程跟晶粒大小有密切關係。雖然減薄薄膜可達至控制晶粒體積大小的效果，但同時也令有序化溫度提高。

另一方面，我們把炭離子注入到磁性薄膜中。跟其他薄膜比較，被離子注入的薄膜有著差不多的矯頑力值和較小的晶粒。在 X-射線衍射圖中峰強的比例表明注入的樣品是長程有序的，同時解釋了即使小的晶粒也具有較強的矯頑力。

此外，研究了不同成分薄膜由於改變 FePt 分割層 C/Cu 的厚度對此產生的影響.

同時化學有序度強烈依賴於添加分割層的厚度。在 FePt-C 當中 fcc-fct 相變隨著分割層厚度增加而遞減。但在 FePt-Cu 當中，當加入薄的 Cu 分割層至 FePt 層之中時，化學有序度達到最大。這表明相變增強在這兩種樣品當中的機制是不同的。

# *Acknowledgements*

It is a pleasure to thank many people who made this thesis possible.

First of all, I am very grateful to my supervisor, Professor S. P. Wong, for his guidance, encouragement and support during my study. Thanks also for his financial support for a year before my study.

Appreciation also goes to Professor J. B. Xu and Professor Aaron H. P. Ho for their invaluable advice for my research work.

Moreover, I must thank Dr. W. Y. Cheung, Dr. N. Ke and Mr. W. K. Chan for their advice and great help in sample preparation and characterization. They contributed a lot in this work. Special thanks to Dr. M. F. Chiah for his patient guidance in the beginning of my study.

Together with my lab mates, Mr. C. F. Chow, Mr. W. C. Law, Mr. K. C. Lo, Mr. S. W. Tsang, Ms. W. Y. Luk, Mr. H. Wang, Ms. Judith Roller, Mr. L. Wang, Mr. X. F. Wang, Mr. J. An, Mr. S. Y. Wu, Mr. X. H. Liu, Mr K. Xue, Mr. M. Zhu, Mr. X. J. Yu, Mr. C. L. Wong, Mr. K. H. Cheng and Mr K. W. Lo, I had an enjoyable research environment and many valuable discussions.

Finally, I like to say "多謝" to my parents, grandma, grandpa, Henry and Wendy for their love, support and understanding. Special words to Crete: "Danke fuer dein Verstaendnis".

# *Table of Contents*

# *List of Figures*

# *List of Tables*

# *Chapter 1*

# *Introduction*

## 1.1 Overview

Introduced in 1957 by IBM, the random access method of accounting and control (RAMAC) was the first hard disk drive. It consisted of 50 magnetic disks of 24-inch in diameter. The storage capacity of this system was 5 MB with the data rate of 12.5 kB/s. It's areal density is only 0.002 $Mb/in^2$, and the slider / disk spacing was about 20 micrometers. About 50 years later, the IBM "Travelstar 80GN" drive has 2.5 inch disks with 80,000 MB capacity and 350 Mb/sec data transfer rate. Areal density of 70,000 $Mb/in^2$ is achieved by antiferromagnetic coupled (AFC) technology. The spacing between the disk and the sliders with heads working on magneto-resistive principles is only about a few dozens nanometers! In fact, this drive is not the newest and the best, it just was randomly chosen to make one point that there was a huge progress in the field of hard disk drive (HDD) technology in the past 50 years. [1]

The introduction of magnetoresistive (MR) and giant magnetoresistive (GMR) heads in 1990's has greatly catalyzed the rapid development of hard disk drive in the past decade. In March 2005, the Hitachi Global Storage Technologies demonstrated an areal density of 230 gigabits per square inch ($Gb/in^2$) on perpendicular recording technology [1]. The rapid development and great demand from world-wide business and individual user in magnetic data storage over the past decade have led to intensive research effort in ultra high density recording media with areal density more than $100Gb/in^2$.

## 1.2 Conventional recording

Longitudinal magnetic recording technology has been dominating the hard disk drive industry for nearly 50 years. Under this technology, the magnetization of each bit is aligned parallel to the platter surface. Shown in Fig. 1.1 is the schematic showing the working principle of longitudinal recording [1].

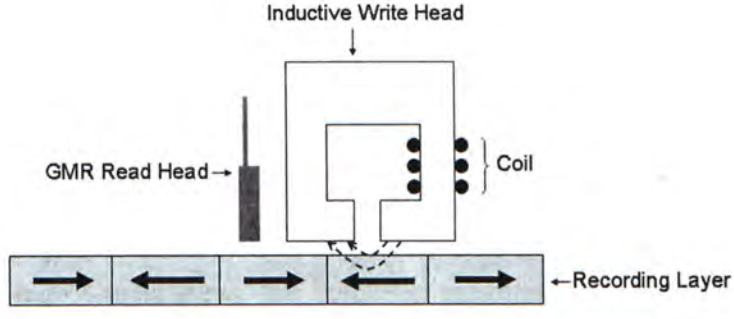


Fig. 1.1 Working principle of longitudinal recording

In longitudinal recording, the magnetization of each bit is aligned parallel or anti-parallel to the direction in which the head is moving relative to the disc. Each bit is approximately made up of 100 magnetic grains. Co-based alloys with the h.c.p. crystal structure are widely used as the recording media. Various alloy additions to the Co (Cr, Ta, Pt, etc) change some of the intrinsic magnetic properties of the alloy.

## 1.3 Superparamagnetism

To increase areal density, as well as overall storage capacity, in longitudinal recording, the data bits on a disc must be made smaller and put closer together. However, there is limitation on the shrinkage of bit size. If individual bit becomes too small, the magnetic energy holding the bit in place may also become so small that thermal

energy can cause it to demagnetize. This phenomenon is known as superparamagnetism. Shown in Fig. 1.2 is a schematic showing this phenomenon.

The recording media can be modeled as assemblies of single-domain, isolated or weakly coupled particles with uniaxial anisotropy which magnetization reversal is achieved by coherent rotation. Based on the Stoner-Wolfarth model [2], in the absence of an external field H, the activation energy barriers is determined by the anisotropy energy density $K_u$ and the particle volume V

$$E_B \cong K_u V \qquad (1.1)$$

At sufficiently high temperatures, the magnetic anisotropy energy barriers of the single-domain particles are overcome by thermal energy $k_BT$ where $k_B$ is Boltzman constant and T is temperature. Under these conditions the magnetic vector of each particle is not fixed but fluctuates rapidly in the directions of particle magnetic moment.

If every bit size, so as the particle volume V, has to be reduced to a certain dimension, the activation energy barrier $E_B$ will be too small that is comparable to thermal energy given in room temperature. Then the magnetic information stored in the recording media can be easily affected by thermal fluctuation and causing data loss. For Co-based media used in present longitudinal recording, such as CoPtCr, $K_u = 2x10^6$ erg/cm$^3$. It cannot satisfy the above requirement if the grain size becomes smaller than 10 nm at room temperature [3].

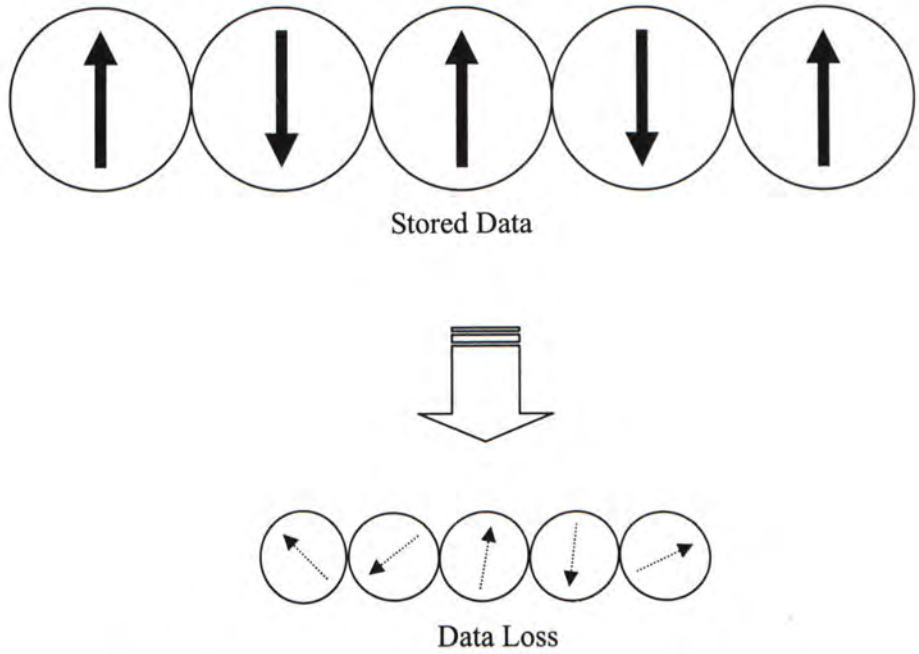


Fig. 1.2 Superparamagnetism: thermal energy causes data loss when grain size is small

## 1.4 Possible solutions

The exact areal density at which the superparamagnetic effect occurs, or the so-called superparamegnetic limit, has been changed by scientists and researchers from time to time. The limit was believed to be 25 megabits per square inch in the 1970's. But the truth is that the limit has been pushed forward several times through innovations in laboratories, those limits have moved forward dramatically. Today, the highest areal density with longitudinal recording is more than 100 gigabits per square inch. But no matter how much effort is put to increase the areal density, the problem of thermal instability will sooner or later comes. However, there are several possible solutions to move the superparamegnetic limit further, as well as to make it vanishes by using brand new idea for magnetic recoding.

### 1.4.1 Perpendicular recording

In perpendicular recording, the magnetization of each bit is aligned vertically such that they are perpendicular to the disk surface. Shown in Fig. 1.3 is the schematic showing the working principle of the perpendicular recording.

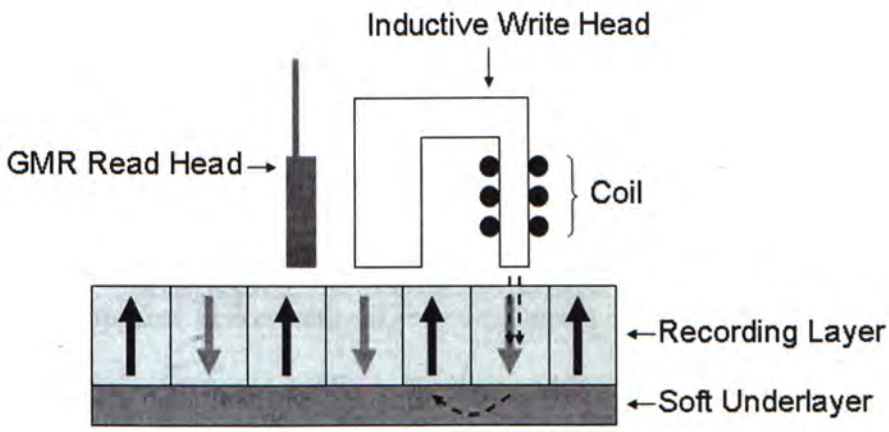


Fig. 1.3 Working principle of perpendicular recording

As shown in Fig. 1.1, the magnetization of each bit is aligned parallel to the surface of the platter in longitudinal recording. In the interface of two bits with opposite magnetization, the field lines repel each other, making it unstable against thermal fluctuation.

In perpendicular recording, the magnetization of each bit is aligned vertically. The magnetizations of adjacent bits not only don't repel each other, but also stabilize each other by completing the field lines. This geometry is the key to making the bits smaller without superparamagnetism causing them to lose their memory.

### 1.4.2 Patterned media

In conventional media, each data bit is made of about 100 nano-scale magnetic grains randomly chosen form the recording media. The boundary between bits may not be a sharply cut and may be blurred by thermal fluctuation, causing data loss.

In patterned media, the recording media is made up of a matrix of many small islands. Each data bit is an isolated magnetic island. The boundaries between adjacent bits are now clearly defined and the problem of blurring boundary vanishes.

Since we no longer need on the order of 100 grains per bit, but just one single grain-sized switching volume, density can be increased by roughly two orders magnitude compared to conventional recording media. Since each island is a single magnetic domain, patterned media is thermally stable, even at densities far higher than can be achieved with conventional media.

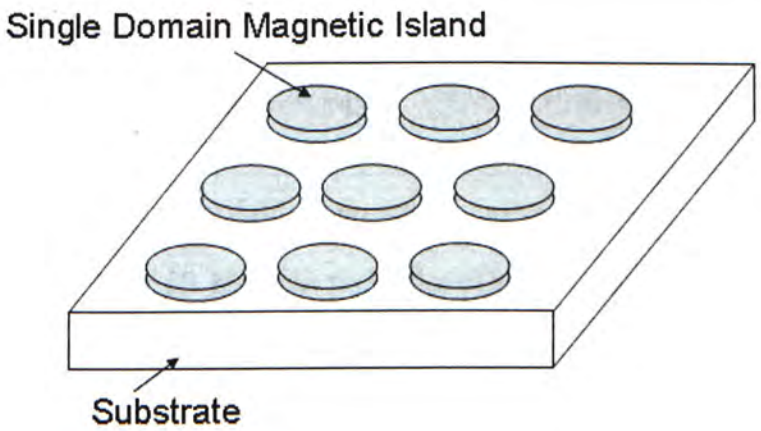


Fig. 1.4 Patterned media

### 1.4.3 High Ku material for recording media

The superparamagnetic effect tells us that when product of the grain volume $V$ and its anisotropy energy $K_u$ fall below a certain value, the magnetization of that grain can flip spontaneously. If a significant fraction of the grains on the disk flip spontaneously, the data stored on the disk erases itself. Since we need to keep reducing size (and therefore $V$) to record at higher densities, one way to maintain thermal stability would be to increase $K_u$. Shown in Table 1.1 is a summary of magnetic properties of different materials [3-6].

| Alloy system | Materials | $K_u$ ($10^7$ erg/cm$^3$) | $M_s$ (emu/cm$^3$) | $D_p$ (nm) |
|---|---|---|---|---|
| Co alloy | CoPtCr | 0.2 | 298 | 10.4 |
| | Co | 0.45 | 1400 | 8.0 |
| | $Co_3Pt$ | 2.0 | 1100 | 4.8 |
| | | | | |
| $L1_0$ phases | FePd | 1.8 | 1100 | 5.0 |
| | FePt | 6.6-10 | 1140 | 3.3-2.8 |
| | CoPt | 4.9 | 800 | 3.6 |
| | MnAl | 1.7 | 560 | 5.1 |
| | | | | |
| Rare-earth Transition metals | $Fe_{14}Nd_2B$ | 4.6 | 1270 | 3.7 |
| | $SmCo_5$ | 11-20 | 910 | 2.7-2.2 |

*$D_p$ is the smallest thermally stable grain size

Table 1.1 Magnetic properties of various materials

High uniaxial magnetocrystalline anisotropy ($K_u$) materials are attractive for ultra-high-density magnetic recording media application, since they can provide smaller thermally stable grains. Prominent candidates include fct or $L1_0$ phases of near-equiatomic composition intermetallic compounds of CoPt, FePt, and rare-earth transition metals of $Co_5Sm$, PrCo and $Nd_2Fe_{14}B$. Recently, FePt attracts great research

interest due to the high magnetocrystalline anisotropy ($K_u$–$7x10^7 erg/cc$) of its ordered tetragonal $L1_0$ phase. Normally, post-annealing at temperatures higher than 600°C is needed to achieve the $L1_0$ phase. The high temperature process is not desirable for the industry. So, great effort has been put to lower the ordering temperature of the desired phase. Examples of such researches will be given in next section.

### 1.5 FePt-based material research

There are two phases of FePt, namely, face centered-cubic (fcc) and face-centered-tetragonal (fct) phases [7-9]. Shown in Fig. 1.5(a) is the structure of the fct phase, which is chemically ordered from the a-c plane. The fcc chemically disordered phase is shown in Fig 1.5(b)

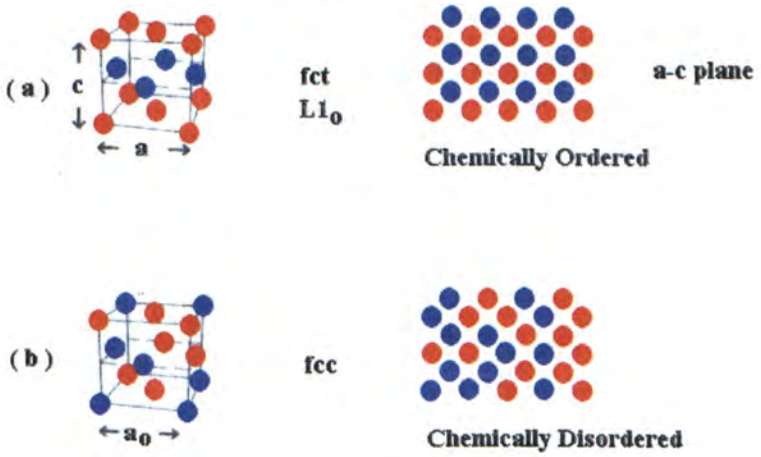


Fig. 1.5 Schematic of (a) chemically ordered fct phase and (b) chemically disordered fcc phase

In the bulk material, equi-composition FePt forms a chemically ordered fct structure below 1300°C, where there are alternating atomic planes of Pt and Fe along the c axis. The chemical ordering drives a tetragonal distortion in the unit cell, and in bulk FePt, c/a= 0.96, where c is the lattice parameter along the chemical order direction and a is the lattice parameter orthogonal to this [10]. However, in thin films, films deposited

near room temperature adopt a disordered fcc (high energy) phase. A high-temperature ($\geq$600°C) treatment such as thermal annealing or high temperature deposition is necessary to overcome the energy barrier to obtain the ordered fct (low energy) phase with high $K_u$[11].

For fct superstructures, there are two kinds of positions, which are designated α and β sites [12]. For ideal equiatomic composition and perfect long-range ordering, the α sites of FePt are all occupied by Fe atoms and the β sites by Pt atoms. The red and blue dots in Fig. 1.5a are representing the α and β sites respectively. The uniaxial ordering in a fct FePt films can be described by a long range order (LRO) parameter *S*, which is defined as [13-14]

$$S = 2(r_\alpha - x_{Fe}) = 2(r_\beta - x_{Pt}) \qquad (1.2)$$

where $x_{Fe}$ and $x_{Pt}$ are the atomic fractions of Fe and Pt, and $r_\alpha$ and $r_\beta$ are the fractions of the α and β sites occupied by the correct atom, respectively.

For fully ordered equiatiomic FePt alloy, $x_{Fe} = x_{Pt} = 0.5$, $r_\alpha = r_\beta = 1$, then $S = 1$. Parameter S can be obtained from the ratio of the integrated XRD intensities of the fundamental ($I_{001}$) and superlattice ($I_{002}$) reflections [5].

The literature predicted the media for future ultra-high density longitudinal recording should have the following properties [3,15]:

1. Coercivity of about 4 kOe~5 kOe, since the common writing field is about 5 kOe in longitudinal recording
2. Weakly exchange-coupled grains with size of < 10 nm and with the preferred in-plane orientation.

The high ordering temperature (>600°C) of FePt fct phase is a major problem in its application for ultra-high density recording media. Not only the high temperature is not favorable for industrial process, but also the high temperature process leads to particle coalescence and loss of particle positional order. Particle coalescence leads to increased particle size, which defeats the objective of making smaller grains for higher areal recording density. Therefore, there are intensive research efforts to lower the processing temperature of FePt in order to apply the high $K_u$ material for commercial ultra-high density recording. Several studies reported that the addition of Cu, Ag, Au, C or Zr in FePt greatly reduced the ordering temperature to moderate temperatures [16-18]. Also, Ag or MgO underlayers were used to reduce the FePt ordering temperature due to the strain effect [18-19]. Fe/Pt multilayer film structure has also been proved to be able to lower the processing temperature [20]. On the other hand, in combined use of 130 keV He ions and simultaneous heating at 280°C led to atomic displacements and atomic rearrangement together with lattice relaxation, Ravelosona et al. [21] have successfully applying ion irradiation method to lower the ordering temperature of FePt films.

Recently in our laboratory, Chiah has investigated the influence of C and Cu additives on the $L1_0$ ordering and grain growth of the multilayer-deposited FePt films prepared by filtered vacuum arc deposition [22]. His results showed that with the C or Cu additives the ordering temperature can be reduced down to 350 °C and 300 °C respectively. However, the grain sizes of the ordered films are all larger than 10 nm, which is too large for ultra-high density recording with low noise.

## 1.6 Project goal

In Chiah's work, it was demonstrated that for multilayer FePt film prepared by filtered vacuum arc deposition with C or Cu as additives a lower ordering temperature of fct phase was achieved. However at the same time the grain size became too large and was not suitable for practical applications. The present work is a follow-up of Chiah's work. We shall adopt the multi-layer deposition approach and to study how the layer thickness and other processing parameters will affect the microstructures and magnetic properties of these films. The ultimate goal is to see if films with the desirable properties suitable for high density magnetic recording medium applications could be achieved. In particular, FePt-C and FePt-Cu multilayer films with different composition and film thickness were prepared by filtered vacuum arc deposition. In addition, a post-deposition ion-implantation process is adopted for some samples. The samples were characterized using a number of techniques including Rutherford backscattering spectrometry (RBS), x-ray diffraction (XRD), vibrating sample magnetometery (VSM), and transmission electron microscopy (TEM). In chapter 2, the details of the sample preparation and characterization will be described. In chapter 3 results and discussions of the FePt-C films will be given and those of FePt-Cu films will be discussed in chapter 4. In the final chapter, a summary of the main research results and suggestions for future work will be given.

**Reference**

[1] http://www.hitachigst.com

[2] E.C. Stoner and E.P. Wohlfarth, Trans. Roy. Soc., vol. A240, 599 (1948)

[3] D.Weller, et al., IEEE Trans. Mag. 36, 10 (2000)

[5] H.Wang and S.P. Wong, "Preparation, Structure, and Properties of Magnetic Nanocompostie Films", in Magnetic nanostructures, edited by Hari Singh Nalwa, ASP (2002)

[6] D. Weller, A.Moser, IEEE Trans. Magn. 35, 4423 (2000)

[7] A. Ceboolada, R.F. C. Farrow, M.F. Tony, " Structure and Magnetic Properties of Chemically Ordered Magnetic Binary Alloys in Thin Film Form", in Magnetic nanostructures, edited by Hari Singh Nalwa, ASP (2002)

[8] R.A. Ristau, et al., J. Appl. Phys. **86**, 4527 (1999)

[9] N.I. Vlasova, G.S. Kandaurova, et al., J. Magn. Magn. Mater. **222**,138 (2000)

[10] A. Cebollada, R.F.C. Farrow and M.F. Toney, in Magnetic Nanostructures, edited by H.S. Nalwa (American Scientific, Stevenson Ranch, CA, 2002)

[11] Michael F. Toney, Wen-Yaung Lee, et al., J. Appl. Phys. **93**, 9902 (2003)

[12] C. Chen, O. Kitakami, et al., J. Appl. Phys. **87**, 6947 (2000)

[13] B.E. Warren, "X-ray Diffraction", Dover, New York (1990)

[14] A. Cebollada, D.Weller, et al., Phys.Rev.B: Solid State **50**, 3419 (1994)

[15] S.H. Charp, Pu Ling Lu, et al., IEEE Trans. Magn., **33**, 978 (1997)

[16] T. Maeda *et al.*, Appl. Phys. Lett. **80**, 2147 (2002)

[17] S.R.Lee *et al.*, Appl. Phys. Lett. **78**, 4001 (2001)

[18] Y.N.Hsu *et al.*, J. Appl. Phys. **89**, 7068 (2001)

[19] R.F.C.Farrow *et al.*, J. Appl. Phys. **79**, 5967 (1996)

[20] Yasushi Endo *et al.*, J. Appl. Phys. **89**, 7065 (2001)

[21] D. Ravelosona, C. Chappert, et al., Appl. Phys. Lett. **76**, 236 (2000)

[22] M.F.Chiah, "Characterization of Magnetic Nanocomposite Thin Films for High Density Recording Prepared by Pulsed Filtered Vacuum Arc Deposition", Ph.D. thesis, The Chinese University of Hong Kong (2004)

# Chapter 2

# *Sample Preparation and Characterization Techniques*

In this chapter, principle of the deposition system used in this project, namely pulsed filtered vacuum arc deposition (PFVAD), will be given in detail. It is then followed by the details of sample preparation processes and conditions. Furthermore, several characterization techniques employed in this work will also be briefly described. These include Rutherford backscattering spectrometry (RBS) for film composition determination, x-ray diffraction (XRD) to study the structure, vibrating sample magnetometery (VSM) to measure the magnetic properties, and transmission electron microscopy (TEM) for high resolution structural analysis.

## 2.1 Pulsed filtered vacuum arc deposition (PFVAD)

Shown in Fig. 2.1 is a schematic diagram of the pulsed filtered vacuum arc deposition system (PFVAD). The main chamber is equipped with three filtered arc plasma sources so that three different species of plasmas can be provided simultaneously for deposition. The high density plasma of cathode material is produced by vacuum arc discharge. Ions are then guided through a bent magnetic filter to deposit on the substrate in the vacuum chamber. The composition and thickness of the films can be precisely controlled by monitoring the integrated charges arriving at the sample holder from the arc sources.

The sample holder is designed to have six positions (1-6) as shown in the figure. When the holder is stretched out, deposition of material in source number 1, 2 and 3 can be done by setting the holder in position 1, 3 and 5 respectively. When the holder

is at the centre, co-deposition of two or three materials can be done depending on the holder position. Position 2 and position 4 are facing the middle of two sources, so co-deposition of two materials can be done. Position 6 is facing source number 2, as it is located in the chamber centre, co-deposition of three materials can be carried out in this position.

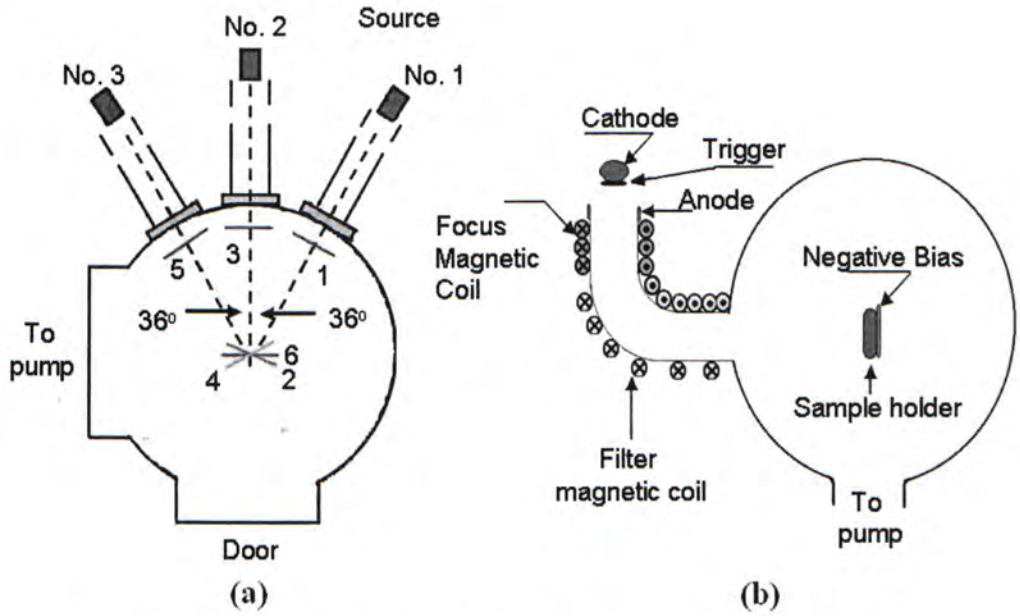


Fig. 2.1 Schematic of the PFVAD system; (a) top-view; (b) side-view.

When the arc is initiated by a high voltage pulse trigger and sustained between the solid cathode and the cylindrical anode, there are cathode spots produced at discrete, minute areas across on the cathode surface. The cathode spot may be regarded as a micrometer sized source of neutral plasma which, in the absence of external fields, moves across the cathode surface in a random manner. It ranges from 1 to 20 um in diameter and is an intense source of photons, electrons, metal atoms, and micrometer sized droplets of the cathode material. Electron-atom collisions result in the formation of positive ions in a region close to the cathode spot surface.

The pressure within the cathode spot is extremely high, up to $10^{10}$Pa [1]. Driven by the intense pressure gradient, the dense plasma rapidly expands into the vacuum or low-pressure gas ambient. Ions are accelerated by the combined forces of the pressure gradient, local electric fields, and electron-ion friction. It has been found that the final ion velocity for all cathode materials is about 1-2x$10^4$m/s, corresponding to ion energies of 20 -200eV depending on the ion mass [1].

Focus magnetic field is employed to sweep the spots over the cathode surface in order to provide for more uniform cathode erosion and to focus the plasma from the source. The concentrated heat flux and the bombardment of ions under electric field at the cathode surface form microscopic liquid pools and then form droplets or so-called macro-particles which are ranged from 0.1 um to 10 um in dimensions. If the macro-particles become entrained in the plasma stream and arrive at the substrate surface, they can cause serious contamination to the films deposited such as inclusion and pinhole defects. So a conventional method, curved magnetic filtering technique is used to reduce macro-particles from the vacuum arc plasma in order to drastically reduce the macro-particle contamination of the films. The underlying principle of filtering is that the macro-particles travel in nearly straight lines due to their inertia while the plasma can be guided to a substrate location which is out of line-of-sight to the cathode spot. Because of their light mass, and by Lorentz force, electrons will move basically along the magnetic field lines. Ions are bound to the electron motion by plasma internal electric fields, and consequently the plasma as a whole follows the magnetic field lines.

There are two DC voltage bias supplies available to be connected to the sample holder in the main chamber. One of them can supply a DC voltage of 0-300 V to provide a

negative bias to the substrate for deposition. The other one can supply a negative DC voltage of 0-30 kV for implantation. A three-channel beam current integrator is connected in series to the substrate power circuit to measure the current arriving at the sample holder. Hence the composition and thickness of the films can be precisely controlled by monitoring the integrated charges arriving at the sample holder from the arc sources.

### 2.1.1 Sample preparation

FePt-C and FePt-Cu nanocomposite thin films were prepared by PFVAD on thermally grown $SiO_2$ of 100nm on (100) silicon wafers. The substrate was placed at the centre of the main chamber while the three cathode sources, Fe, Pt and C/Cu were installed separately. To achieve multilayer film structure, the three sources were operated one by one in a well designed sequence. During the operation of each source, the substrate was turned to face the corresponding source by a stepping motor connected with the sample holder. -80 V bias was applied to the substrate during deposition, while negative voltage in kV order 0was used during post-deposition implantation. Thickness of intended deposited layer is monitored by the charge counter in the sample holder, although the actual thickness and composition of the film was determined by RBS. Details of experiment setting are given in Appendix 1.

## 2.2 Rutherford backscattering spectroscopy (RBS)

Rutherford backscattering spectroscopy is a non-destructive method to determine chemical composition as a function of depth and thickness of the samples. The sample under investigation is bombarded with high energy Helium ions. These ions penetrate

the sample and eventually they collide with the atoms in the structure. Some of them will reflect backwards and get out of the sample. Finally these reflected ions are collected by a detector which records their energy. The energy is a function of the depth of the collision and the mass of the target atom. Thus, from the measured energy distribution of the reflected ions, we can deduce the location of the collision and the mass of the target atom. However, RBS is not sensitive for light elements embedded in matrices of hervier elements such as carbon in silicon. Therefore, for films consist of C atoms as one of the components, non-Rutherford backscattering spectrometry (NRBS) was used to determine the C composition. In my work, a beam of 3.5MeV $He^{++}$ ions was used to perform NRBS, which have a non-Rutherford resonance scattering cross-section with C atoms so that the sensibility of detecting carbon is greatly enhanced in order to achieve a more accurate film composition and thickness determination.

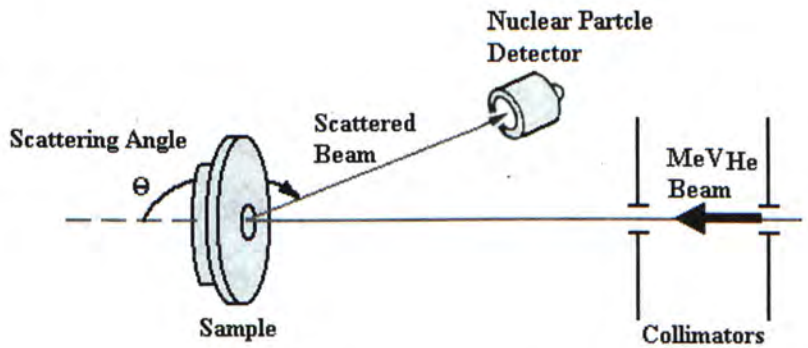


Fig. 2.2 Schematic of RBS measurement

In this project, non-Rutherford backscattering spectrometry (NRBS) was performed with a 2MV tandem accelerator. A beam of 3.5MeV $He^{++}$ ions was irradiated an incident angle of $7^{o}$ to the normal of the film plane and the backscattered $He^{++}$ ions were collected at a scattering angle of $170^{o}$ with respect to the incident direction. To

determine the thickness and composition of the film, the NRBS spectra were fitted and simulated by the computer software SIMNRA [2]. Accuracy of thickness determined by fitting can be found in Appendix 2.

## 2.3 X-ray diffraction (XRD)

X-ray diffraction (XRD) is a non-destructive method to characterize crystalline materials. It provides structural information of the investigated samples, such as crystal structure, phase and texture. X-ray diffraction peaks are produced by constructive interference of the monochromatic beam scattered from each set of lattice planes at specific angles. The peak intensities are determined by the atomic decoration within the lattice planes. Consequently, the x-ray diffraction pattern is the fingerprint of periodic atomic arrangements in a given material. An on-line search of a standard database for x-ray powder diffraction pattern enables quick phase identification for a large variety of crystalline samples [3].

In this project, grazing angle configuration has been employed. Shown in Fig. 2.3 is the schematic diagram of the XRD configuration used. The grazing incidence angle was fixed at $1^{\circ}$ and the $2\theta$ angle ranged from $20^{\circ}$ to $60^{\circ}$. The patterns were obtained by a standard x-ray diffractometer with a Cu anode.

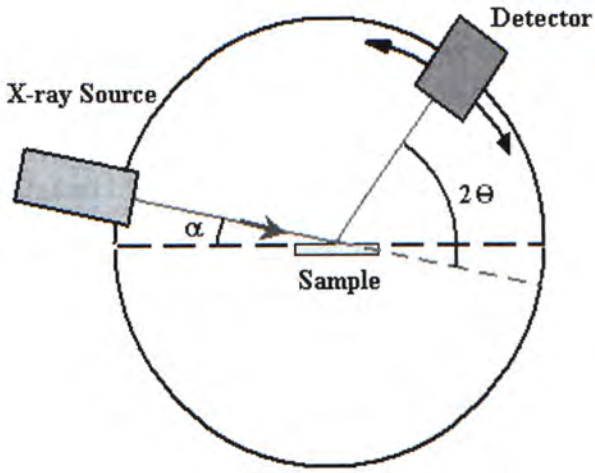


Fig. 2.3 Schematic diagram of an x-ray-diffractometer in the α-2θ mode configuration

The grain size can be determined by the Scherrer formula, which is shown below [4]:

$$D = \frac{K\lambda}{W\cos\theta} \qquad (2.1)$$

where $D$ is the grain size, $K$ is the constant 0.9 if half-maximum width is used, $\lambda$ is the wavelength of the x-ray source ( in this work the Cu-K$\alpha$ line of wavelength 0.15405nm is used), $W$ is the full-width-half-maximum of the peak and $\theta$ is the diffraction angle. Generally, when grain size is larger than 100 nm, the grain size-related peak broadening is not significant. But the broadening becomes significant when the size is around 10 nm. By repeated experiments, the accuracy of grain size estimation is within 0.1 nm in sample with grain size of 6.5 nm.

## 2.4 Vibrating sample magnetometery (VSM)

Vibrating sample magnetometery was employed to determine the magnetic properties of samples. Sample is placed inside a uniform magnetic field and is made to undergo sinusoidal motion by mechanical vibration. This motion of the magnetized sample

creates magnetic flux change. This induces voltage in the pick-up coils, which is proportional to the magnetic moment of the sample.

In this project, the Oxford Instruments Vibrating Sample Magnetometer with a 9 Tesla superconducting magnet with a maximum sensitivity of about $10^{-6}$ emu was employed. The sample under investigation was mounted on a plastic sample holder attached to a carbon fiber rod. A mechanical vibrator is connected with the carbon fiber rod to provide vertical vibration in 55 Hz with amplitude 1.5 mm. A uniformly applied magnetic field up to 9 Tesla is provided by a superconducting magnet immersed in liquid helium. The magnetic moment of the sample is obtained by the pick-up coils surrounding the sample holder during the vibrating motion at the presence of the applied field. Shown in Fig. 2.4 is a schematic diagram of the VSM and it's controlling system [5 ].

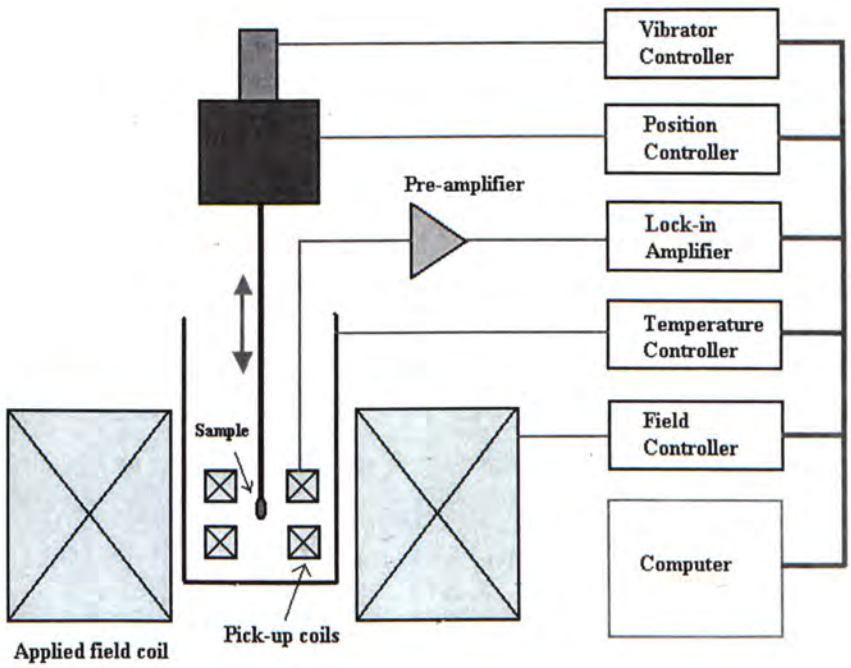


Fig. 2.4 Schematic of VSM measurement [5]

## 2.5 Transmission electron microscopy (TEM)

Transmission electron microscopy is a powerful technique to investigate the sample's structural properties with ultra high magnification. An electron beam, instead of visible light in conventional optical microscope, is employed in TEM to form image of the sample. Because the wavelength of electrons is much smaller than that of light, the resolution attainable for TEM images can be many orders of magnitude higher than that for a light microscope. The image can be in atomic resolution and lattice structure can be identified.

In this project, cross-sectional TEM images of different samples have been obtained in order to provide a clear picture of the grain size distribution and nano-scale structural image.

**Reference**

[1] Specification of PFVAD, Institute of Low Energy Nuclear Physics, Beijing Normal University.

[2] Matej Mayer, SIMNRA Version 4.40, (1997)

[3] Nuffield, E. W., "X-ray diffraction method" (1996)

[4] M. J. Buerger, 'Vector space and its application in crystal-structure investigation', (Wiley, New York 1959)

[5] Specification of Oxford VSM.

# *Chapter 3*

# *Characterization of FePt-C Nanocomposite Thin Film*

In this chapter, the preparation of FePt-C thin films with different total thickness, different spacer thickness and post-deposition implantation will be described. Then characterization of these films by using XRD, VSM and TEM will be discussed.

## 3.1 Experiment design

From Chiah's work [1], multilayer FePt film with carbon additive was found to be able to lower the ordering temperature to 350°C. However, the grain size of the correspondent nanocomposite film is larger than 10 nm, which is too large for ultrahigh density recording media. Therefore it is of interest to explore methods to control the grain growth during thermal treatment. One simple approach is to limit the total film thickness. In Chiah's work, the film thickness was 50 nm. In this project, films with thickness of 25 nm and 10 nm have been prepared and characterized. On the other hand, post-deposition ion-implantation has also been employed and was believed to be able to lower the ordering temperature.

## 3.2 Experiment detail

Multilayer structures were first produced using the PFVAC system. Iron, platinum and carbon layers of various designs were deposited on thermally grown $SiO_2$ films. By monitoring the charge counter of the PFVAD system, thickness of each deposited layer can be precisely controlled. The substrate, silicon wafer with approximately 100 nm thermally grown $SiO_2$, was placed at the centre of the deposition chamber with a negative 80 V DC bias. The iron, platinum and carbon cathode source were operated

alternatively in pulse mode with a 2.5 ms pulse duration and a frequency of 4 pulses/s. No substrate heating is applied during deposition. Shown in Fig. 3.1 is a schematic diagram of one typical multilayer film.

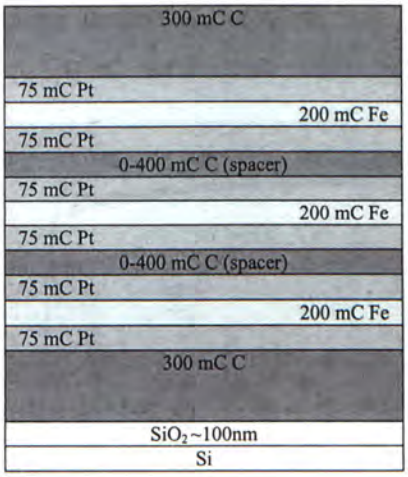


Fig. 3.1 Schematic of a "3-cycle" multilayer FePtC film

The multilayer Fe/Pt films are separated by several carbon spacer layers of different thickness. Besides varying the spacer thickness, total thickness of film have also been varied. Shown in Fig. 3.1 is a schematic for a batch of samples with 3 metal layers to be referred to as the 3-cycle films. There is also another batch of samples consisting of 9 metal layers to be referred to as 9-cycle samples. With these, the composition dependence, as well as total thickness dependence, of fct phase formation in these films were investigated.

Post-deposition carbon ion-implantation into these multilayer films was also performed. The implantation was done in the PFVAD system immediately after deposition. Carbon ions with high energy were obtained by increasing the negative substrate bias voltage from 80 V to kV order.

Thermal annealing was performed in argon atmosphere after deposition or implantation. All films were annealed for 10 minutes at temperatures ranging from 370°C to 670°C. Shown in Fig. 3.2 is a typical temperature-time profile of the rapid thermal processing with a target temperature of 470°C.

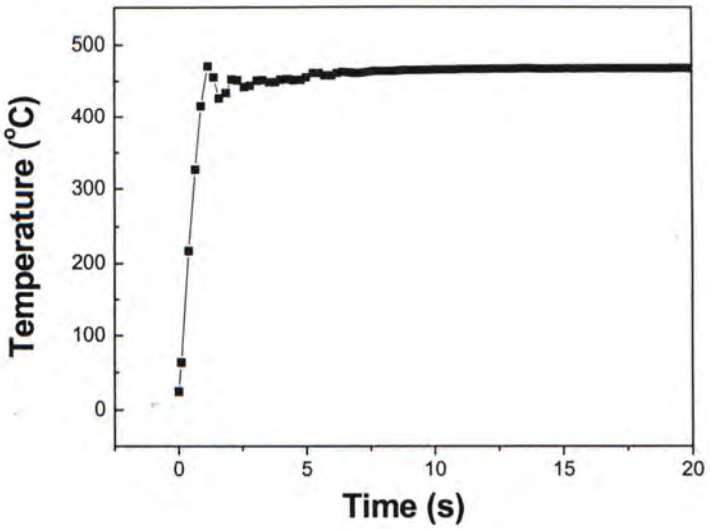


Fig. 3.2 A typical temperature-time profile of the rapid thermal processing

### 3.3 Results and discussion

#### 3.3.1 NRBS measurements

In the PFVAD system, thickness of the deposited film is controlled by charge counters. To ensure repeatability, wafers with the same area were used in each deposition, so that a particular amount of charge for a specific material is corresponds to a particular thickness. To find out the relationship between the accumulated charge and the thickness, 1000 mC (mini Coulomb) of Fe, Pt and C were deposited on $SiO_2$ and their thicknesses were determined by NRBS measurement. Shown in Fig. 3.3 is the NRBS spectrum of this film. The result is tabulated in Table 3.1.

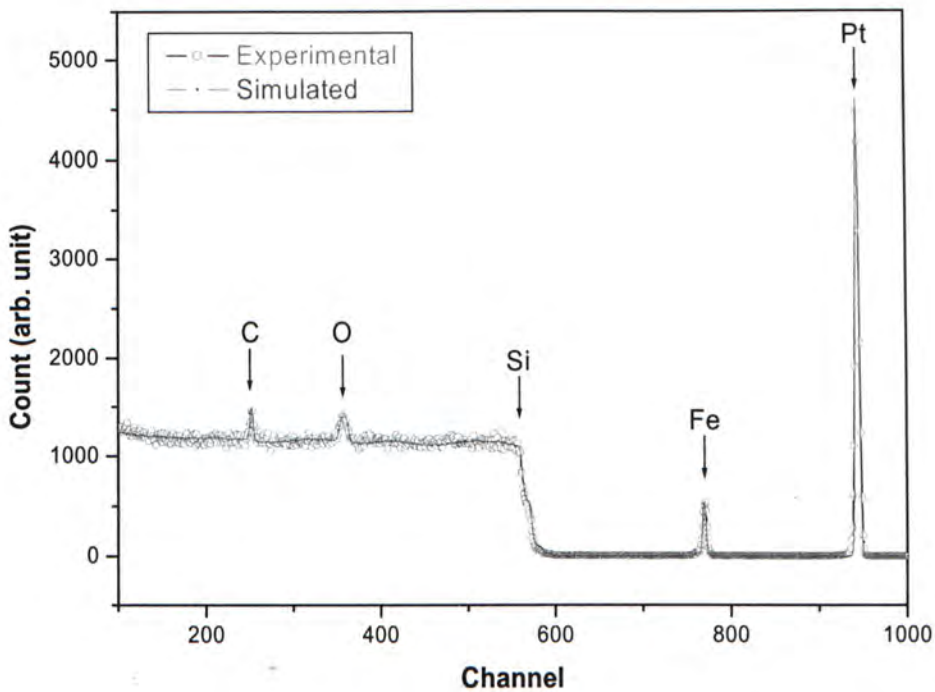


Fig. 3.3 NRBS spectrum of 1000 mC of C, Fe and Pt deposited on $SiO_2$

| | Charge counted (mC) | Thickness (nm) |
|---|---|---|
| Fe | 1000 | 4.1 |
| Pt | 1000 | 4.8 |
| C | 1000 | 6.2 |

Table 3.1 Fitted thickness of the 1000mC C, Fe and Pt film from NRBS spectrum

Based on the charge-to-thickness relationship found, multilayer films with different total thickness and composition were designed and deposited. Shown in Fig. 3.4 is the NRBS spectrum of the as-deposited 3-cycle FePtC multilayer films and the film structure model built from the deposition sequence. The experimental spectrum was

fitted with the model and thickness of each layer was estimated. Shown in Fig. 3.5 is the NRBS spectrum of the as-deposited 9-cycle FePtC films with the corresponding film structure model. The result is tabulated in Table 3.2. The variation in composition is not expected and comparison between different samples has to be careful. Improvement in controlling system during deposition is needed.

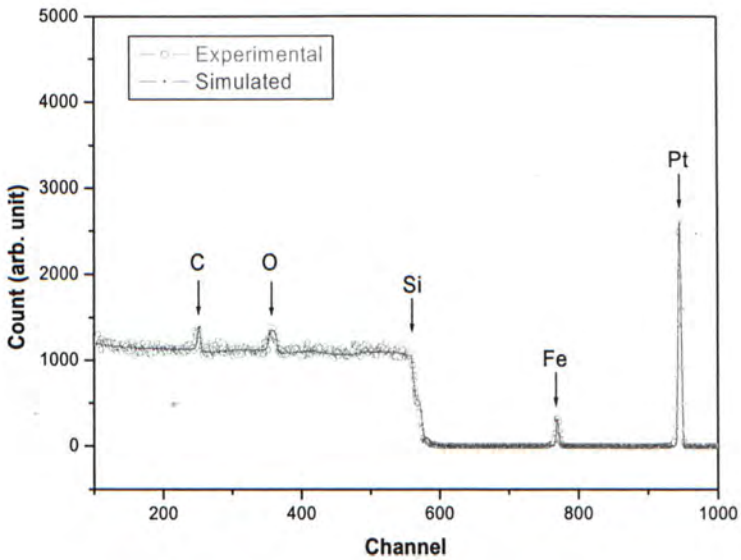


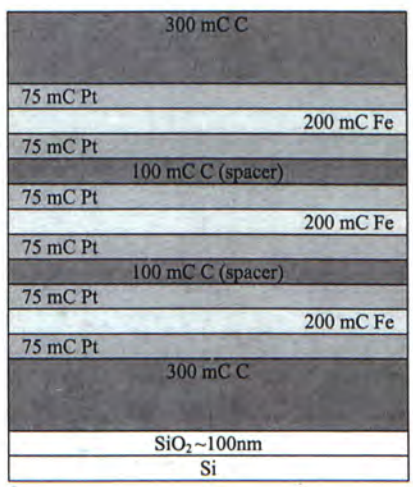


Fig. 3.4 (a) NRBS spectrum of tbe 3-cycle FePtC film with a 100 mC C spacer and (b) the multilayer film model used in fitting

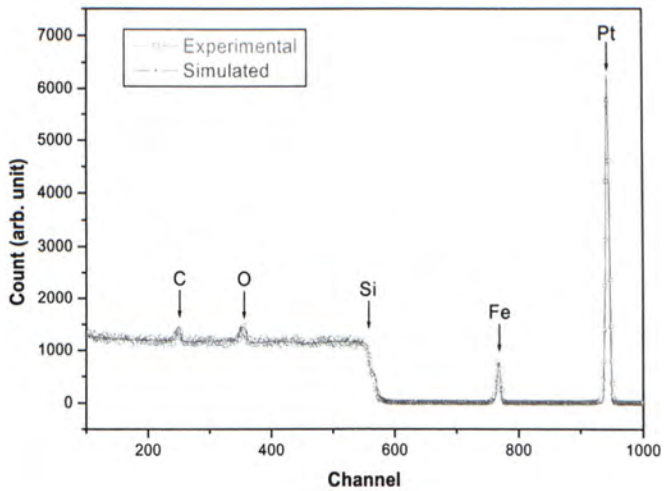


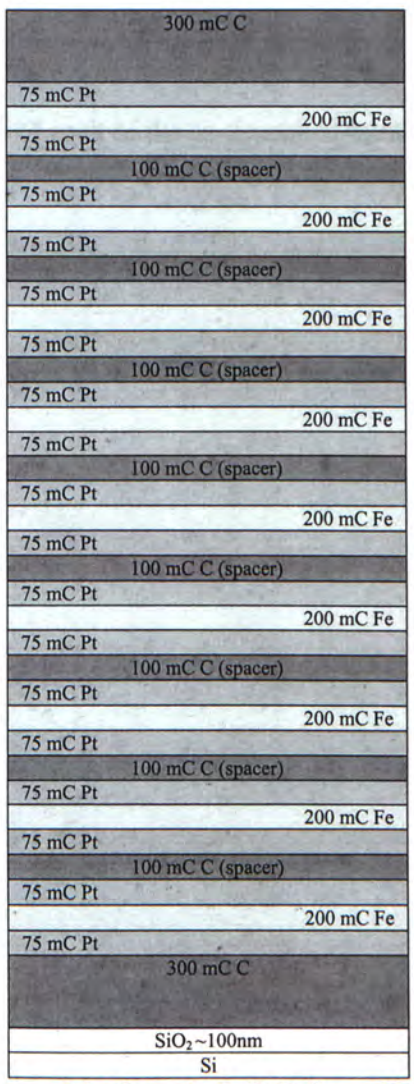


Fig. 3.5 (a) NRBS spectrum of the 9-cycle FePtC film with 100 mC C spacer and (b) the multilayer film model used in the fitting

| | Spacer deposited | Spacer (C) thickness | Pt thickness (75 mC) | Fe thickness (200 mC) | Elemental ratio | Total thickness |
|---|---|---|---|---|---|---|
| 3-cycle | 0mC | 0 | 0.5nm | 0.9nm | $Fe_{24}Pt_{20}C_{56}$ | 9.7nm |
| | 100mC | 0.7nm | 0.5nm | 0.8nm | $Fe_{20}Pt_{18}C_{62}$ | 11.4nm |
| | 200mC | 1.2nm | 0.5nm | 0.9nm | $Fe_{18}Pt_{15}C_{67}$ | 12.6nm |
| | 300mC | 2.0nm | 0.5nm | 0.8nm | $Fe_{15}Pt_{14}C_{71}$ | 13.8nm |
| 9-cycle | 0mC | 0 | 0.4nm | 0.6nm | $Fe_{31}Pt_{35}C_{34}$ | 17.3nm |
| | 100mC | 0.6nm | 0.4nm | 0.9nm | $Fe_{32}Pt_{22}C_{46}$ | 25.4nm |
| | 200mC | 1.2nm | 0.5nm | 0.8nm | $Fe_{26}Pt_{22}C_{52}$ | 27.0nm |

Table 3.2 The fitted results of each of the as-deposited multilayer film from the NRBS spectra

### 3.3.2 XRD measurements

The structural properties of the films were studied by glancing angle x-ray diffractometry with the incident angle of 1°. Shown in Fig. 3.6 are the XRD spectra of the 3-cycle FePtC film with 100mC spacer annealed at various temperatures ranging from 470 to 670 °C for 10 minutes. For the as-deposited film, no superlattice peak is observed, indicating that the film stayed in fcc phase. Upon annealing the film to 570 °C, the superlattice (001), (110) and (201) peaks of FePt can be clearly seen. This implies that the disorder-order transformation in the FePt films has started. Another feature is the overlapping of the fcc (200) and superlattice (002) peaks. When the annealing temperature increased to 670 °C, the superlattice (002) peak moved away from the fcc (200) peak, and the increased intensities of the fct peaks indicates a more complete phase transformation.

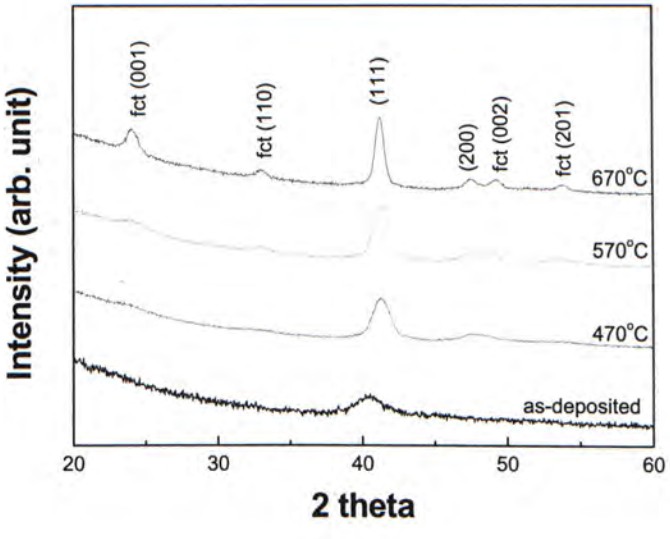


Fig. 3.6 XRD spectra of the 3-cycle FePtC film with a 0.7 nm C spacer annealed at various temperatures for 10 minutes

Shown in Fig. 3.7 are the XRD spectra of the 3-cycle FePtC films annealed at 470°C with different carbon spacer thickness, ranging from 0 to 2.4 nm. The results indicate that the transformation temperature strongly depends on the carbon spacer thickness. For the film without or with thin C spacer layer, they show the presence of fct FePt peaks. This implies the disorder-order transformation has started at this temperature. However, for the film with thicker C spacer thickness, no fct FePt peaks are observed. These suggest that a thicker C spacer layer between the magnetic metal layers tends to prohibit the ordering phase transformation.

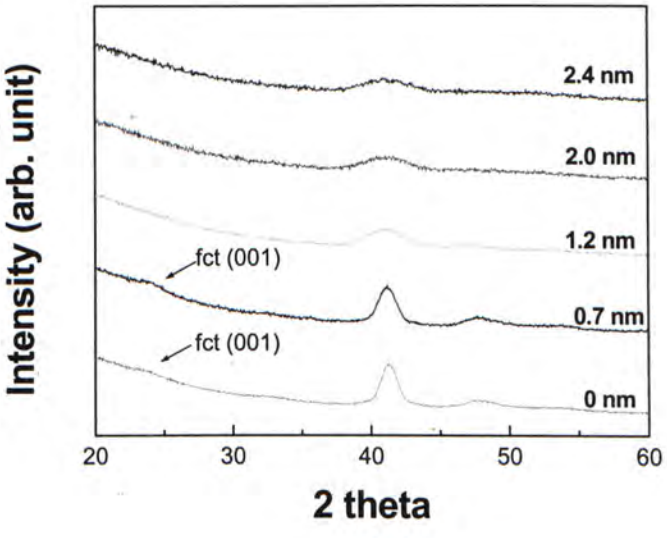


Fig. 3.7 XRD spectra of 3-cycle FePtC films annealed at 470°C with different carbon spacer thickness

Shown in Fig. 3.8 are the XRD patterns of the 9-cycle FePtC film with 100 mC spacer annealed at various temperatures ranging from 370 to 570 °C for 10 minutes.

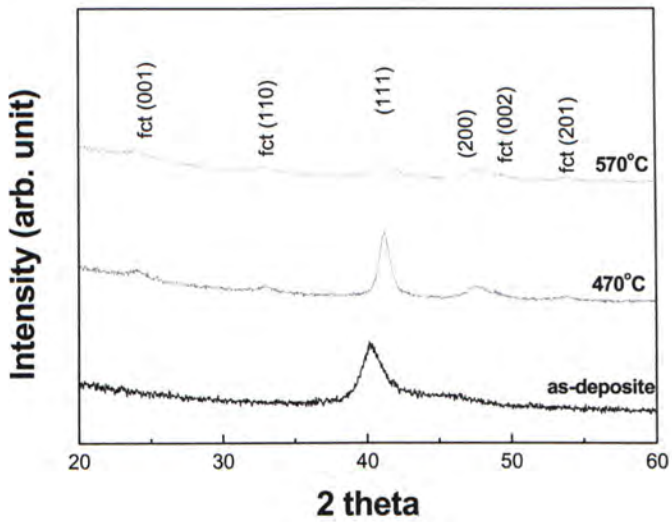


Fig. 3.8 XRD patterns of the 9-cycle FePtC film with 0.6 nm C spacer annealed at various temperatures

When compared with the similar plot for the 3-cycle samples in Fig. 3.6, they show similar trend: fct superlattice peaks appear after annealing and become more significant for higher annealing temperatures. However, under the same annealing temperature, the intensities of the fct peaks of the 9-cycle samples are stronger. It was suggested that the lack of chemical order in thinner films was due to a lack of nucleation sites [3]. Our results are consistent with this reasoning and there are reports of similar findings on the dependence of ordering temperature on film thickness [4].

Shown in Fig. 3.9 are plots of the grain sizes of the 3-cycle and 9-cycle FePtC films against C spacer thickness. The grain sizes were estimated by Scherrer's formula using the FWHM of the (111) peaks. Generally, grain sizes decrease when the C spacer thickness increases. Thicker C spacer may prevent the coalescence of FePt grains in different layers to form larger grains. Grains are isolated in different layers

separated by the thicker carbon layer, resulting in a smaller grain size. On the other hand, when comparing the results for the 3-cycle and 9-cycle FePtC films with the same C spacer thickness, the 9-cycle samples show a larger grain size. This could be due to the fact that there is a larger amount of FePt available in the 9-cycle samples, therefore larger grains could be formed.

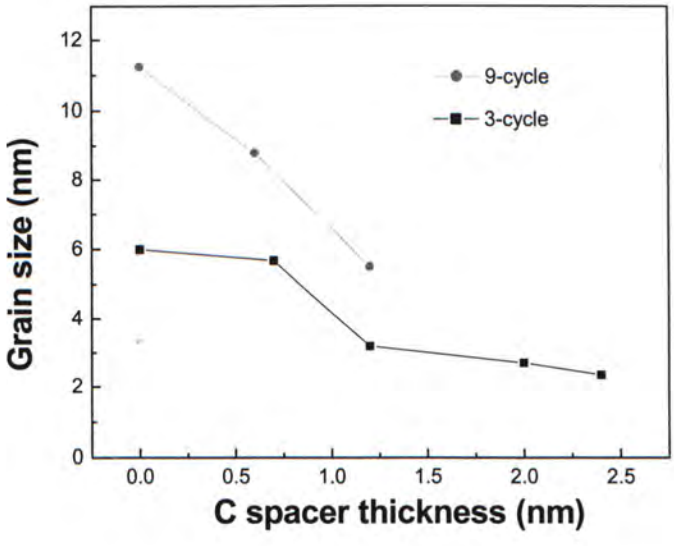


Fig. 3.9 Grain size of the 3-cycle and 9-cycle FePtC samples with different carbon spacer thickness annealed at 470°C

Shown in Fig. 3.10 are the plots of grain size versus annealing temperatures. The grain size increases with annealing temperature as expected because the grain growth rate is higher at higher temperatures. Also, the grains in the 9-cycle samples all have larger sizes than those in the 3-cycle samples under the same heat treatment conditions.

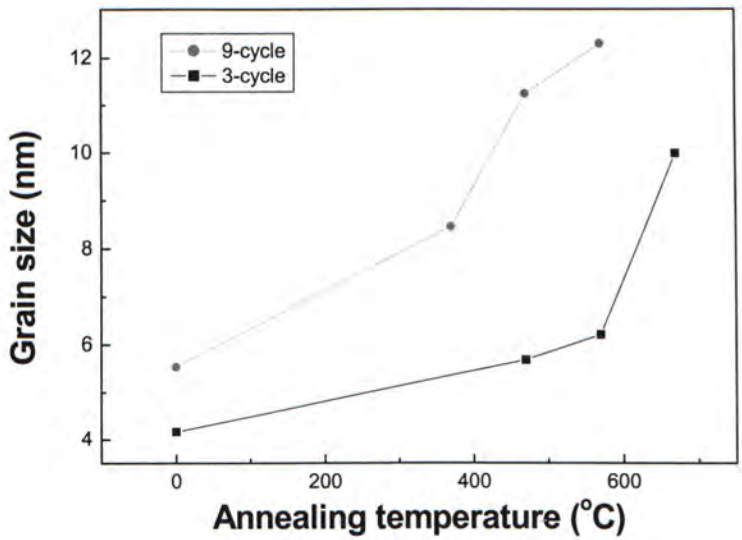


Fig. 3.10 Grain size of the 3-cycle and 9-cycle FePtC samples without carbon spacer after annealing at different temperatures

In summary, at the same annealing temperature, the 9-cycle FePtC samples have larger grain size than the 3-cycle samples have. At the same time, the 9-cycle samples show more complete phase transformation than the corresponding 3-cycle samples. This is consistent with the reported grain size dependence of the phase formation that large grains favor fct phase formation [2]. On one hand, grain growth is limited by reducing the total film thickness, but on the other hand, a higher ordering temperature is required.

Some of the multilayer samples have been implanted with 200 mC carbon ions by increasing the negative bias voltage at the substrate from -80 V to various energies in the 4-14 kV range. Shown in Fig. 3.11 are the XRD spectra and the plot of grain size estimated by Scherrer's formula vs. substrate bias. Generally the implanted samples have smaller grains than the un-implanted one (0 kV) has. It is believed that the post-deposition ion bombardment has led to atomic displacements and produced a lot more

nucleation sites for the ordering transformation, hence leading to enhancements of the phase formation during annealing [5]. As the XRD (001)/(002) peak intensity ratio can provide useful information on the ordering transformation that is highly related to the magnetic properties, we shall further discussed these effects in conjunction with the magnetic properties in the subsequent sections

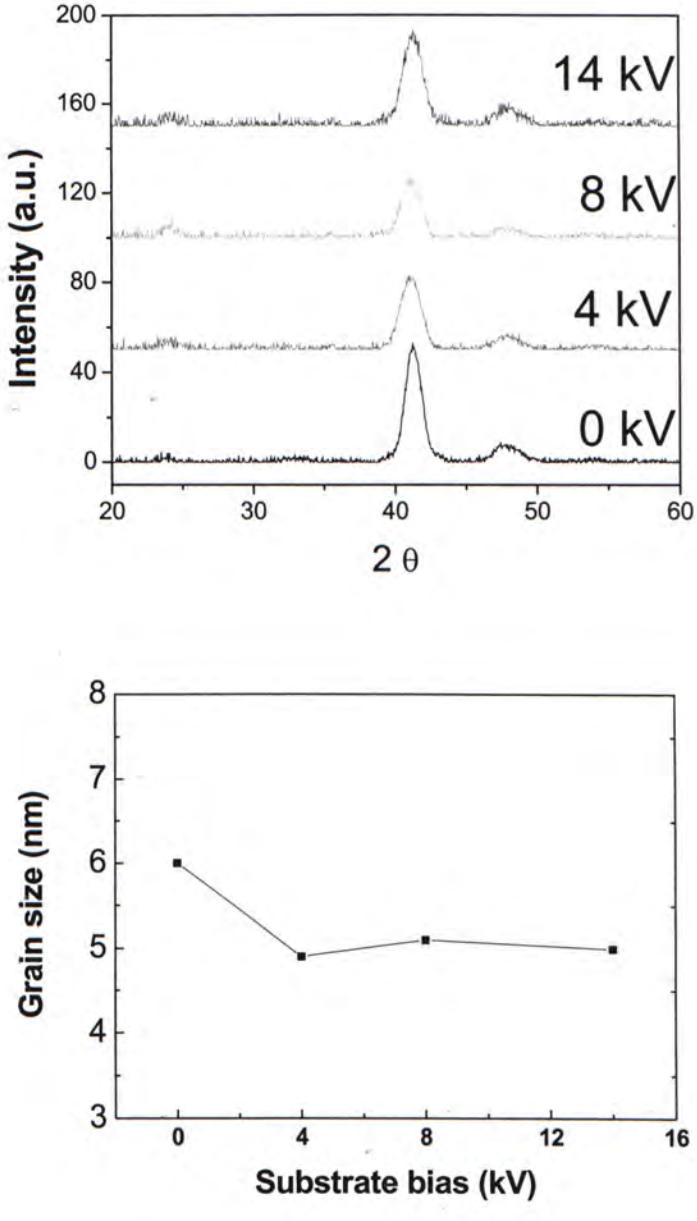


Fig. 3.11 XRD spectra and grain size of implanted samples after annealing at 470°C for 10 minutes versus implantation energy (the data at 0 kV corresponds to the un-implanted sample)

### 3.3.3 VSM measurements

The magnetic properties were studied by vibrating sample magnetometery. Magnetic hysteresis loops were obtained at 300K in the presence of an in-plane applied field. Shown in Fig. 3.12 is the hysteresis loops of 3-cycle FePtC sample with a 0.7 nm carbon spacer layer annealed at various temperatures ranging from 370 to 570 °C for 10 minutes. The saturation magnetization and coercivity as a function of annealing temperature were summarized in Fig. 3.13

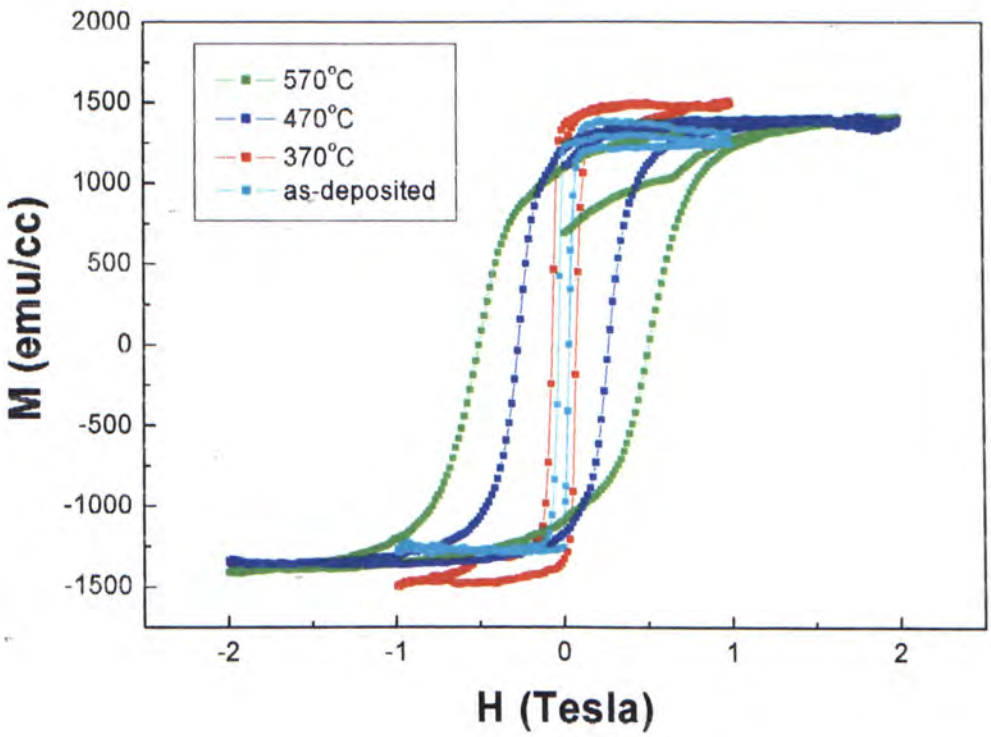


Fig. 3.12 Hysteresis loops of the 3-cycle FePtC samples with a 0.7 nm carbon spacer layer annealed at various temperatures for 10 minutes

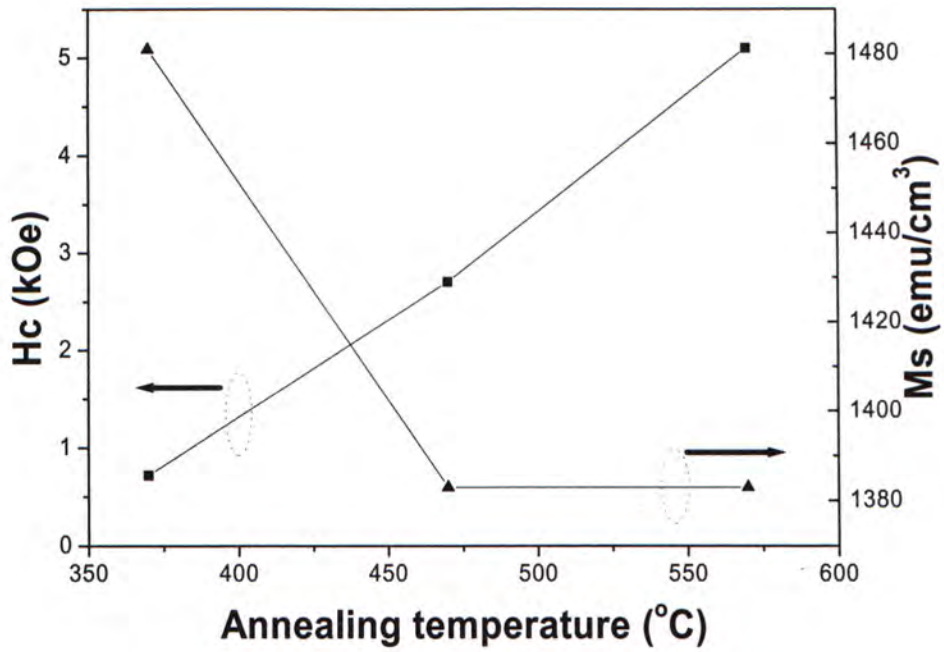


Fig. 3.13 Hc and Ms of the 3-cycle FePtC samples with a 0.7 nm carbon spacer layer annealed at various temperatures for 10 minutes

The coercivity of the as-deposited sample is only 0.3 kOe, which shows the film is in the weak FePt fcc phase structure. The coercivity starts to increase to 0.7 kOe when the film was annealed in 370°C. Then it increases sharply to 3.7 kOe when the annealing temperature is raised to 470°C. The rapid increase indicates that the disorder-order transformation started and the magnetically hard FePt fct phase started to form. A further increase of annealing temperature to 570°C led to a more complete fcc to fct phase transition and a rather high coercivity of 5.1 kOe. The magnetic properties obtained by VSM show strong correlations with the phase information obtained by XRD measurements. The higher the annealing temperature, the clearer are the fct superlattice peaks in the XRD spectra, and also the larger the coercivity.

Shown in Fig. 3.14 are the hysteresis loops of 3-cycles FePtC samples annealed at 470°C with different carbon spacer thickness, ranging from 0 to 1.8 nm. The saturation magnetization and coercivity as a function of carbon spacer thickness were summarized in Fig. 3.15.

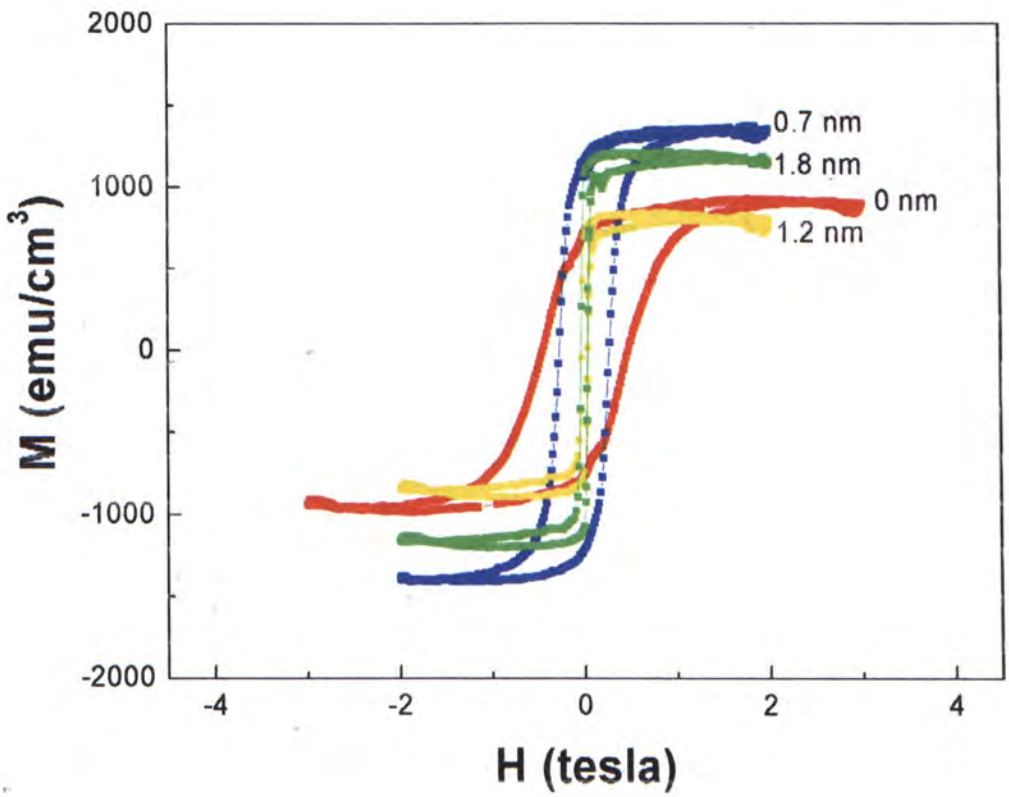


Fig. 3.14 Hysteresis loops of 3-cycles FePtC annealed at 470°C with different carbon spacer thickness

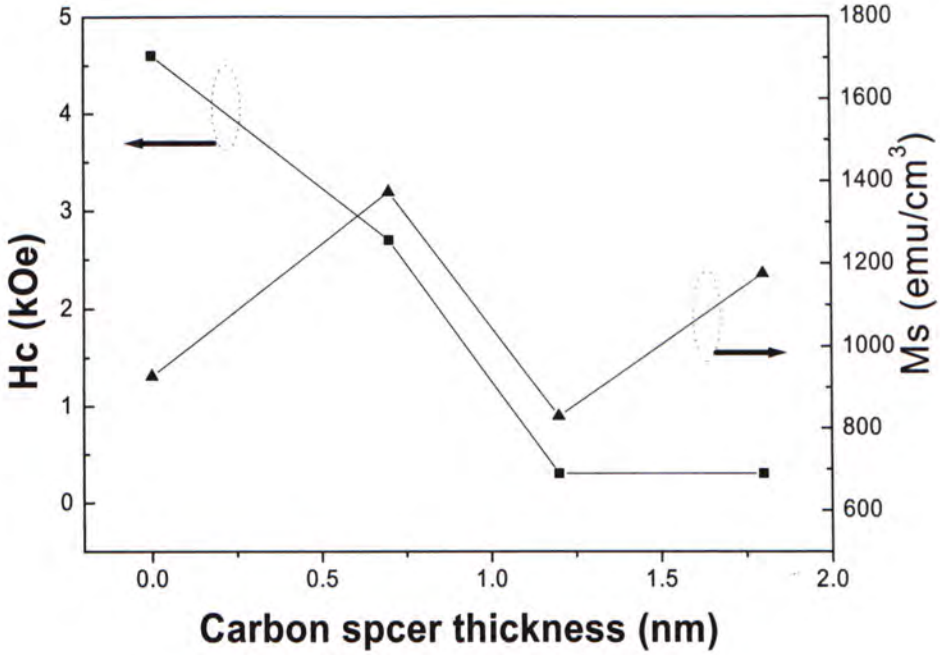


Fig. 3.15 Hc and Ms of the 3-cycles FePtC annealed at 470°C with different carbon spacer thickness

The coercivities are decreasing when carbon spacer thickness increases. This agrees with the XRD results shown before. In the films without carbon spacer (0 nm) or with thin spacer (0.6 nm), fct superlattice peaks present in their XRD spectra, and their coercivities are relatively large (4.6 and 2.7 kOe respectively). Both the presence of fct peaks and large coercivity are the results of disorder-order transformation. The as-deposited magnetically soft fcc phase begins to transform to hard fct phase at 470°C in these two samples. On the other hand, the coercivities of samples with 1.2 nm and 1.8 nm C spacer are both 0.3 kOe only. This shows that the FePt still remains in fcc phase, which is also supported by the absence of superlattice peak in XRD spectra.

Shown in Fig. 3.16 are the hysteresis loops of the 9-cycle FePtC samples with a 0.6 nm carbon spacer annealed at various temperatures ranging from 370 to 570 °C for 10 minutes. The saturation magnetization and coercivity as a function of annealing temperature were summarized in Fig. 3.17

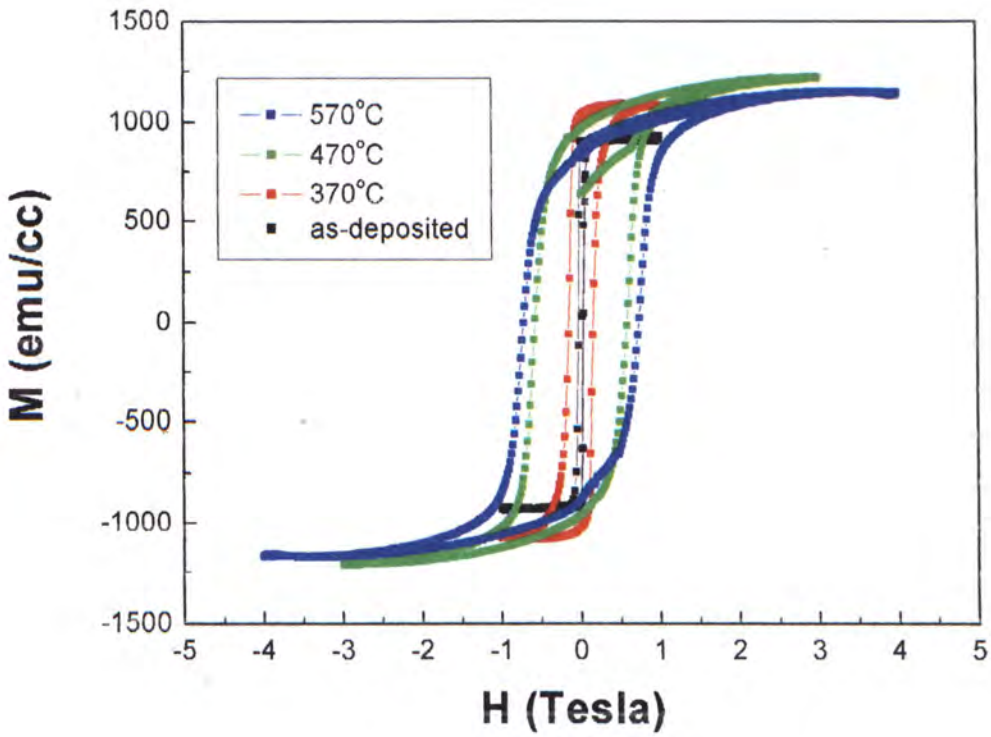


Fig. 3.16 Hysteresis loops of the 9-cycle FePtC with a 0.6 nm carbon spacer annealed at various temperatures for 10 minutes

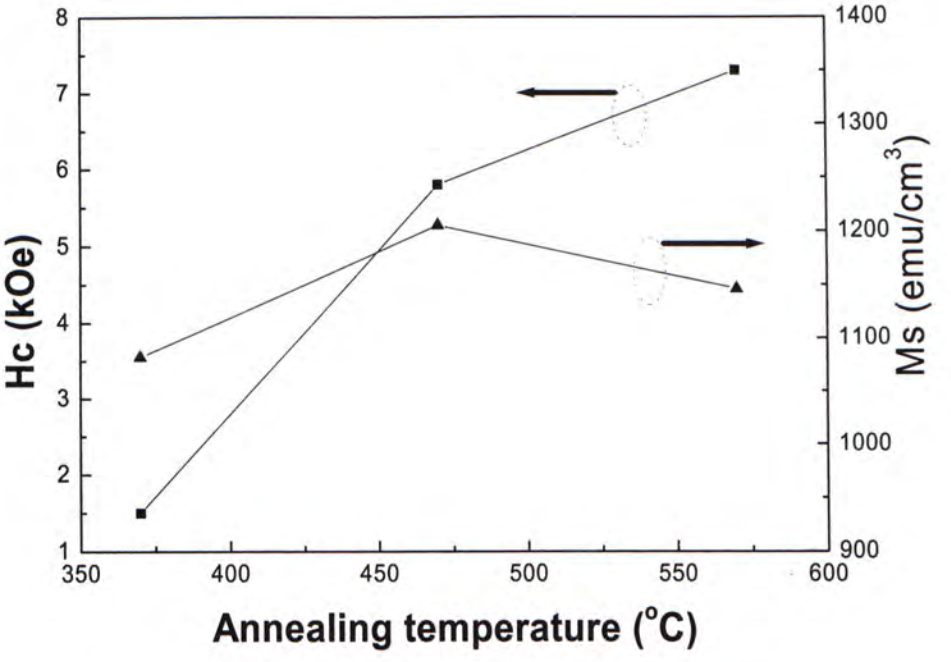


Fig. 3.17 Hc and Ms of the 9-cycle FePtC with a 0.6 nm carbon spacer annealed at various temperatures for 10 minutes

The coercivity of the as-deposited sample is only 0.3 kOe. This shows that the FePt grains in the film are in the magnetically soft fcc phase. The coercivity starts to increase to 1.5 kOe when the film was annealed in 370°C. Then it increases sharply to 5.8 kOe when the annealing temperature is raised to 470°C. A further increase of annealing temperature to 570°C caused a more complete fcc to fct phase transition with 7.3 kOe coercivity. The increase of coercivity with annealing temperature shows similar trend as in the 3-cycle samples. But generally the coercivities of the 9-cycle samples are larger than those of the 3-cycle samples for the same annealing temperature. A clearer picture will be shown and discussed later in this chapter.

Shown in Fig. 3.18 is the hysteresis loops of the 9-cycles FePtC samples annealed at 470°C with different carbon spacer thickness, ranging from 0 to 1.2 nm. The

saturation magnetization and coercivity as a function of carbon spacer thickness were summarized in Fig. 3.19.

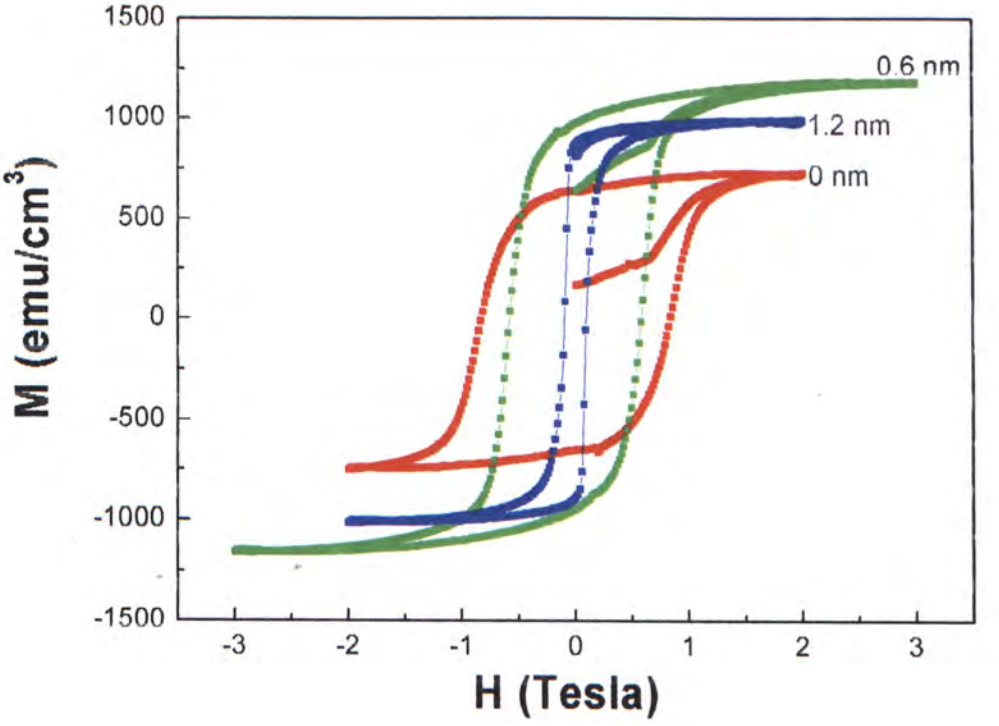


Fig. 3.18 hysteresis loops of the 9-cycles FePtC annealed at 470°C with different carbon spacer thickness

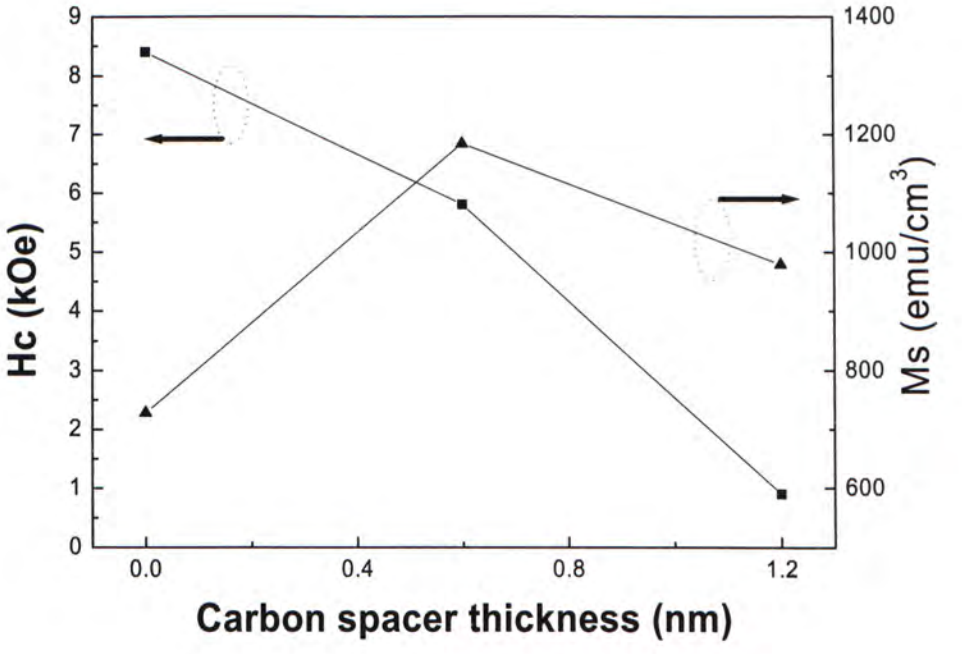


Fig. 3.19 Hc and Ms of the 9-cycles FePtC annealed at 470°C with different carbon spacer thickness

The coercivities are decreasing when carbon spacer thickness increases. The sample without a C spacer has the largest coercivity of 8.4 kOe. The increase of spacer thickness to 0.6nm causes the decrease of coercivity to 5.8 kOe. It further reduces to 0.9 kOe in the sample with the thickest spacer of 1.2 nm. This shows a similar trend as in the 3-cycle samples. Moreover, with the same spacer thickness, all the coercivity values of the 9-cycle samples are larger.

From the above, both the 3-cycle and 9-cycle samples showed the same trend in their magnetic properties: (i) the coercivity increases with annealing temperature, (ii) the coercivity deceases when the C spacer thickness increases. But the 9-cycle samples have larger coercivity values than those of the 3-cycle samples when the spacer

thickness and annealing temperature are the same. For comparison, a plot of the coercivities of these samples versus the C spacer thickness is shown in Fig. 3.20.

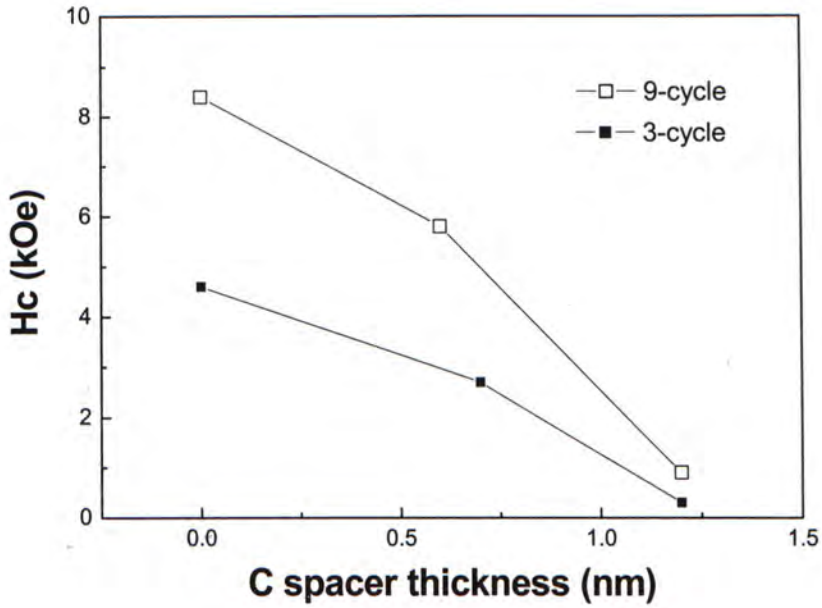


Fig. 3.20 Coercivity of the 3-cycle and 9-cycle FePtC samples annealed at 470°C for 10 minutes versus carbon spacer thickness

This plot shows a similar picture with the plot of grain size against spacer thickness in Fig. 3.9. Both the coercivity and grain size are decreasing with increasing spacer thickness. On the other hand, both coercivity and grain size are larger in 9-cycle samples than in 3-cycle samples. This could be an indication of grain size dependence of FePt fct phase formation.

Regarding the spacer thickness effect, a thicker C spacer will be unfavorable for the FePt grains at the two sides of the spacer to coalesce into a larger grain, hence also unfavorable for the fct phase formation. As a result, the coercivity is smaller. Regarding the total thickness effect, a smaller total film thickness will also limits the

grain growth in the vertical dimension, hence the overall grain size is also limited. Therefore the coercivities are smaller in the 3-cycle samples.

### 3.3.4 Some preliminary results on effects of post-deposition implantation

We have also performed some preliminary experiments to explore the effects of post-deposition implantation to the properties of these films. Shown in Fig. 3.21 is a plot of the coercivities of the multilayer samples implanted by carbon ions with a total implantation charge of 200 mC corresponding to a dose of $1.56 \times 10^{16}$ C ions/cm$^2$. The coercivity of the un-implanted sample (0 kV) is also shown for comparison. The coercivities of the as-implanted samples and the un-implanted sample before annealing all show a small coercivity of 0.3 kOe. After annealed at 470°C, the coercivities increase. It might be tempted to expect that the coercivities of the implanted samples will be larger than that of the un-implanted one, due to the extra energy brought by the implanted ions to the film for disorder-order transformation. But as shown in Fig. 3.21, there is no obvious correlation between the coercivities and the implantation energy. Rather, all of them are in the same order. But from XRD results, as shown in Fig. 3.11, it is found that generally the implanted samples have smaller grain size. As we noted earlier that larger grains are favorable for the fct phase formation, larger grains will usually have larger coercivity for films with otherwise similar conditions. In this case, the implanted samples are having similar coercivity with smaller grain size when compared with the un-implanted one. This post-deposition implantation effect of reducing the final grain size while achieving a similar coercivity certainly suggests for more flexibility in the processing of these magnetic thin films to fine tune their magnetic and structural properties to suit the application requirements. It is also noticed that the grain size does not seem to depend

on the implantation energy. These results could be discussed as follows. The as-deposited film is only partially crystallized as evidenced from the XRD results. As the implant dose is the same for this batch of samples and at these implantation energies, most of the implanted C atoms will not stay in the deposited magnetic thin films, the implanted C atoms will serve to introduce a lot more nucleation sites for the crystallization. Hence the implanted films will result in more grains with smaller size and are expected to have narrower size distribution according to classical nucleation and growth theory. At the same time, the number of nucleation sites for the ordering transformation is also enhanced probably due to the additional energy transfer processes among atoms during the implantation. Hence the ordering is more complete, as indicated by the XRD (001)/(002) peak intensity ratio, at the same annealing temperature compared with the un-implanted films.

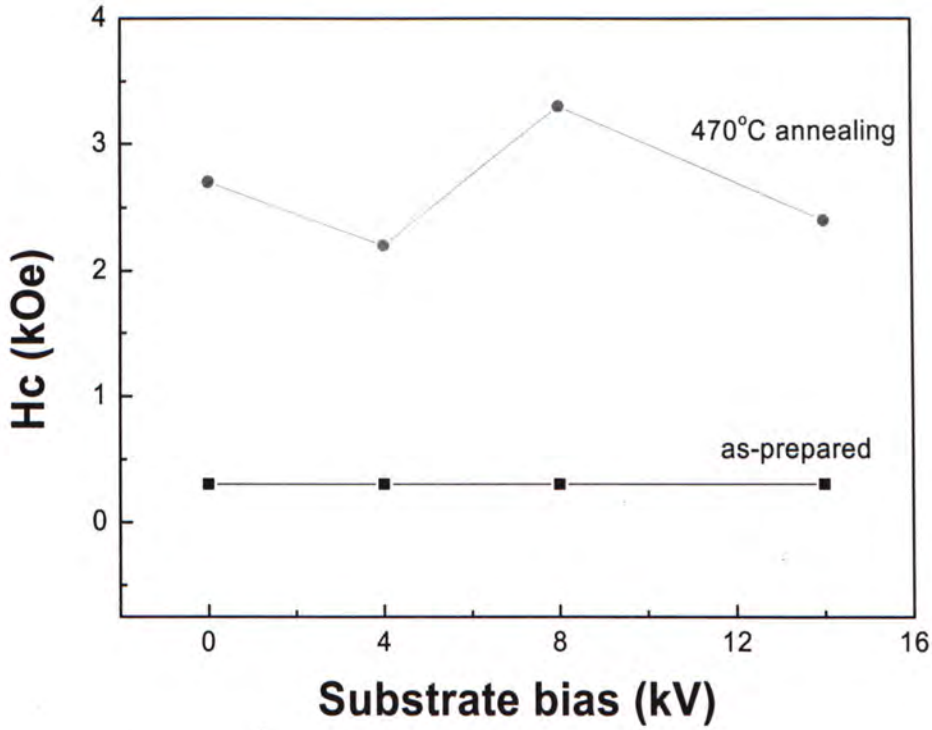


Fig. 3.21 Coercivity of the C implanted multilayer samples versus the substrate bias voltage. The results for the un-implanted sample (indicated as 0 kV) are also included for comparison

### 3.3.5 TEM images

Shown in Fig. 3.22 are the cross-sectional TEM images of the as-deposited 9-cycle samples with 1.2 nm C spacer. From the high resolution image, the 8 spacer layers of C are not uniform in thickness. Rather, there are two main thick layers of carbon with several thinner layers. A possible reason for the non-uniformity of the C layers thickness is that the TEM image was taken 4 months after the sample preparation, during that 4 months time, the C in different layers might diffuse to nucleation sites and form thicker layers while thinning the others. The self-assembly of C into multilayer in thin film at room temperature was also reported by the other group [6].

Shown in Fig. 3.23 is the cross-sectional TEM image of the same sample annealed at 470°C. Only two main C layers left and they are separating the metal layers. The previous thin carbon layers disappeared while the two main C layers became thicker and more solid. This is due to the diffusion of carbon during annealing. The two thick C layers acted as nucleation sites and C in other layers diffused towards them forming thicker continuous carbon layers. Crystallized metal grains are found in different layers.

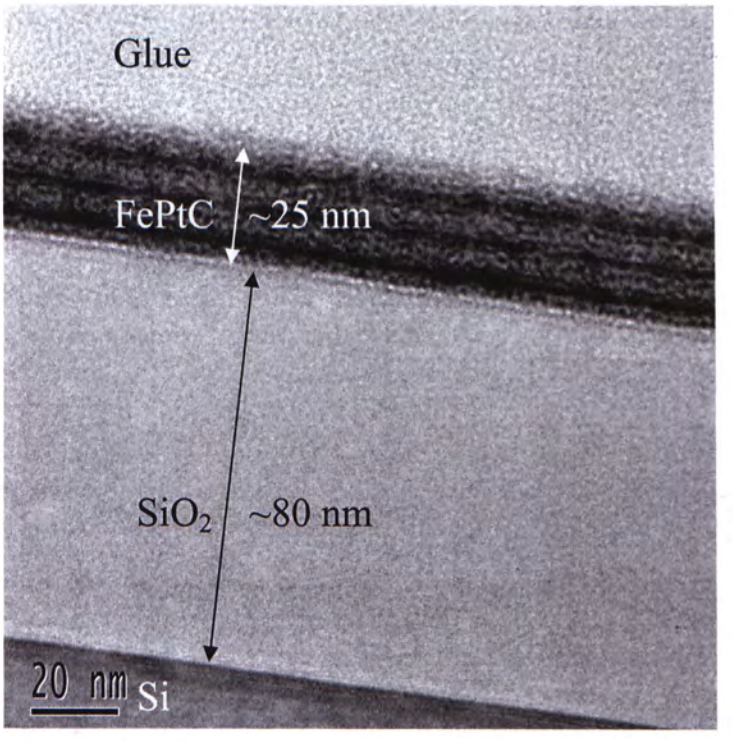


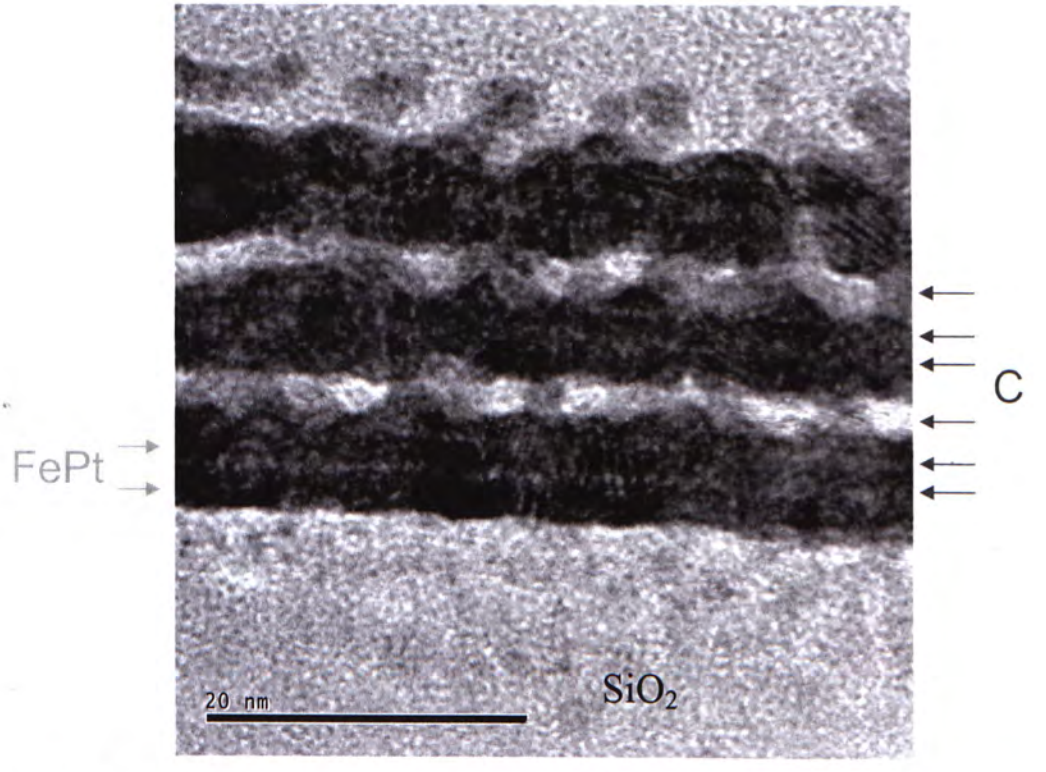


Fig. 3.22 Cross-sectional TEM images of the as-deposited 9-cycle samples with a 1.2 nm C spacer.

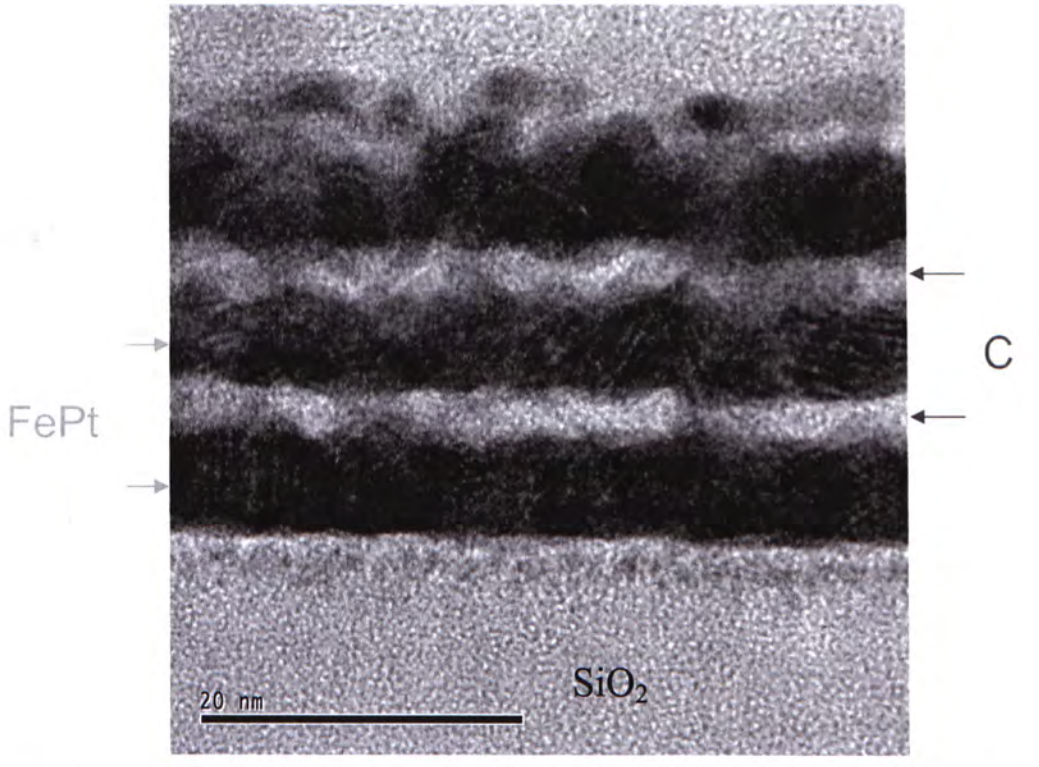


Fig. 3.23 Cross-sectional TEM image of the 9-cycle sample with a 1.2 nm C spacer after annealing at 470°C

### 3.3.6 Overall Discussion

#### 3.3.6.1 Total film thickness effect

Shown in Fig. 3.24 are the plots of coercivity against annealing temperature of different samples. Fig. 3.24(a) shows Chiah's results of his FePtC multilayer samples with ~50 nm film thickness [1]. Fig. 3.24 (b) and (c) are respectively the results of the 9-cycle (~25 nm) samples and 3-cycle (~10 nm) samples of the present work. All the plots are in the same scale and for each graph a horizontal dotted line is inserted at a coercivity of 5kOe for easy comparison. In Chiah's results, the coercivity of the film with the thinnest C spacer ($Fe_{0.41}Pt_{0.38}C_{0.21}$) reaches a value of 5 kOe at an annealing temperature of 350°C. For films with thicker spacer layers, annealing temperatures higher than 500°C were required in order to have the same 5 kOe coercivity. When the total film thickness is reduced to ~25 nm (the 9-cycle samples of this work), as shown in Fig. 3.24(b), the annealing temperature needed for the films to achieve a 5 kOe coercivity became higher. When the film thickness is further reduced to ~10 nm (the 3-cycle samples), as shown in Fig. 3.24(c), the required annealing temperature to achieve the same coercivity rises to 570°C. As the coercivity is highly related to the crystal phase structures of the films, the temperature needed to achieve a certain coercivity value is related to the temperature needed to achieve a certain degree of FePt crystallization in the fct phase. Therefore the above result indicates that the thinner the total thickness, the higher is the temperature required to transform the FePt grains from the magnetically soft fcc phase to the hard fct phase to a certain degree. In general, a thinner film thickness is associated with a higher ordering temperature.

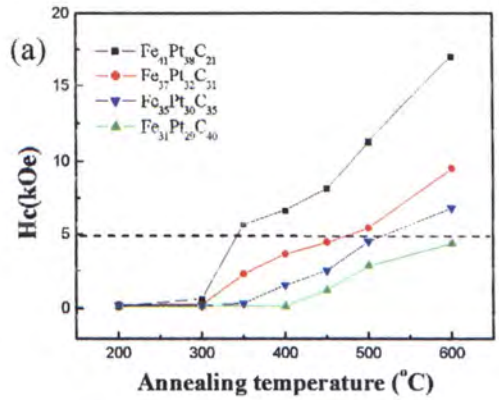


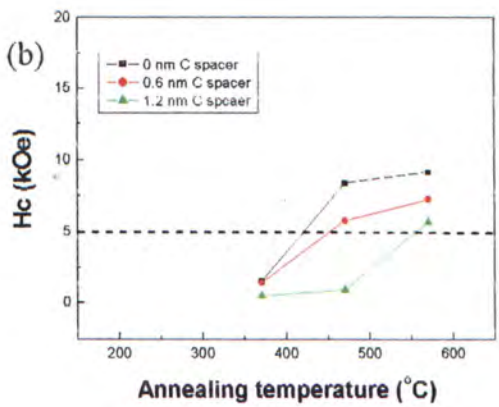


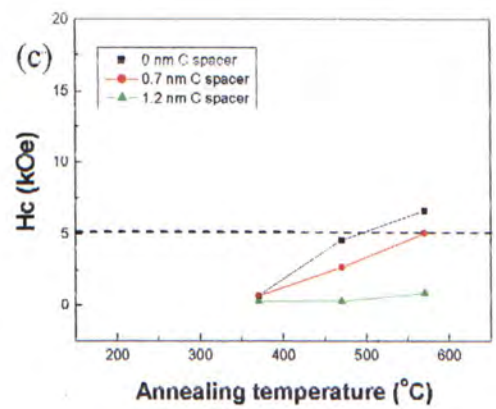


Fig. 3.24 Coercivity of (a) Chiah's 50 nm samples, (b) 9-cycle (~25 nm) samples and (c) 3-cycle (~10 nm) samples versus annealing temperatures

Shown in Fig. 3.25 are the plots of grain size against annealing temperature of different samples. Shown in Fig. 3.25(a) are Chiah's results of his FePtC multilayer samples with ~50 nm film thickness [1] and in Fig. 3.25 (b) and (c) are respectively the results of the 9-cycle (~25 nm) samples and 3-cycle (~10 nm) samples of this work. In each graph a horizontal dotted line is inserted at a grain size of 10 nm for easy comparison. Chiah's results show that the grains grew to larger than 10 nm after annealing at 350-400°C. However the grains are smaller in the 9-cycle samples with similar annealing temperatures. When the film thickness is further reduced (the 3-cycle samples), the grain growth is further suppressed and the grain sizes are well below 10 nm even after annealing at higher temperatures. These results clearly show that grain growth is suppressed by reducing the total film thickness.

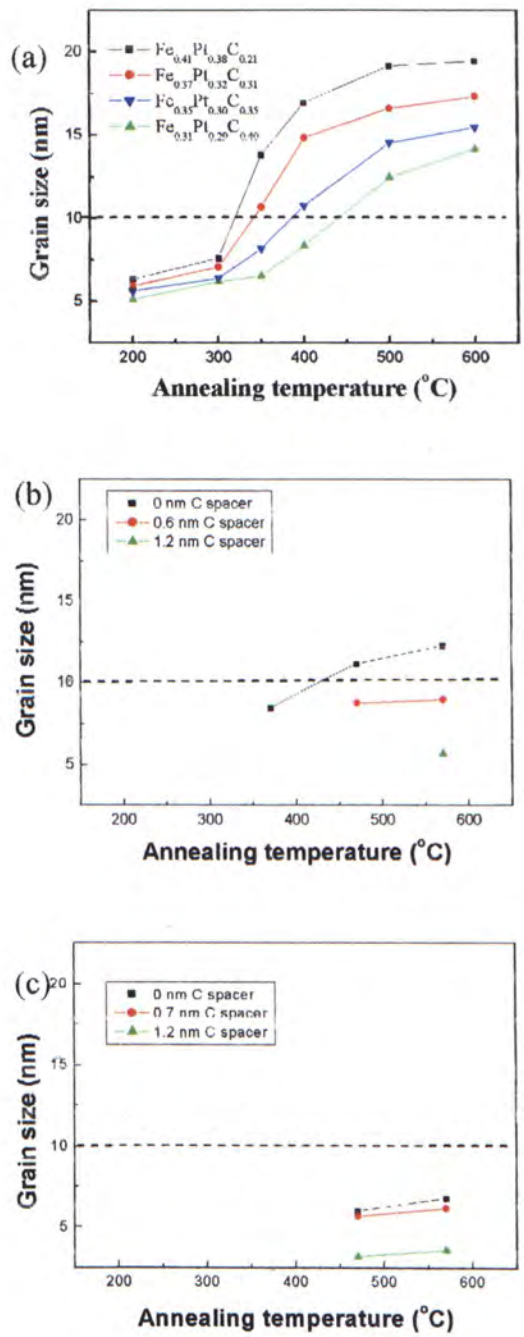


Fig. 3.25 Grain size of (a) Chiah's 50 nm samples, (b) 9-cycle (~25 nm) samples and (c) 3-cycle (~10 nm) samples versus annealing temperatures

From the above, it is seen that grain growth can be successfully suppressed by reducing the film thickness. But at the same time, thinner film needs higher ordering temperature to achieve the same coercivity. These results are obviously related to the grain size dependence of the FePt ordering transformation [1-2]. As a thicker film contains more amount of FePt to form larger grains, it is more favorable to transform into the ordered fct phase.

### 3.3.6.2 Degree of ordering from XRD (001)/(002) peak intensity ratio

The ratio of the (001) superlattice peak to the (002) fundamental peak in XRD spectrum is an indication of the degree of chemical ordering in FePt, i.e. the periodic layer-by-layer arrangement of Fe and Pt atoms. Unfortunately, in many of the XRD spectra obtained for our samples, the (002) peak intensity is too weak and not significant. Therefore only for some samples the XRD peak intensity ratios can be determined and they are tabulated in Table 3.3 for comparison.

| | Sample | Annealing Temperature (°C) | Hc (kOe) | Grain Size (nm) | (001)/(002) |
|---|---|---|---|---|---|
| a | 3-cycle (0.7 nm spacer) | 570 | 5.1 | 6.8 | 1.6 |
| b | Chiah's $Fe_{0.37}Pt_{0.32}C_{0.31}$ | 500 | 5.5 | 16.5 | 1.2 |
| c | 9-cycle (1.2 nm spacer) | 570 | 5.7 | 5.7 | 2.25 |
| d | 9-cycle (0.6 nm spacer) | 470 | 5.8 | 8.8 | 2.1 |
| e | 3-cycle (C implanted at 8kV) | 570 | 6.4 | 5.7 | 3.8 |
| f | Chiah's $Fe_{0.41}Pt_{0.38}C_{0.21}$ | 400 | 6.7 | 17 | 1.9 |
| g | 3-cycle (no spacer) | 570 | 6.7 | 6 | 2.8 |

Table 3.3 Hc, grain size and XRD (001)/(002) peak intensity ratio of various samples

For easy comparison the table is sorted in ascending order of coercivity. In sample (b) and (c), they have similar coercivities while having very different grain sizes. This can be explained by the difference in the (001)/(002) ratio. Although sample (c) has a smaller grain size, the large (001)/(002) ratio indicates that there is better long range order (LRO) inside the grain, which means a more complete fcc-fct phase transformation in this sample. Similar is true when comparing sample (f) and (g). On the other hand, when we compare samples (c) and (e) which have a similar grain size, as the grains in sample (e) have a more complete fcc-fct transformation indicated by the large (001)/(002) ratio, the coercivity is larger. However, larger (001)/(002) ratio does not necessarily mean a larger coercivity. In samples (e) and (f), although there is a big difference in the (001)/(002) ratio, they have similar coercivity. This is because the larger grain size in (f) with a shorter range order can still provide a large coercivity. We may conclude that the coercivity of a sample is decided by both the size of grains and the degree of long range ordering in the grains. In other words, if we regard the degree of long range ordering as the quality of grain, then the coercivity is depending on the size, as well as the quality, of grains.

#### 3.3.6.3 C spacer thickness effect

In both the 3-cycle and 9-cycle samples, the coercivity decreases with increasing C spacer thickness. Although the films without a spacer have the largest coercivities, the grain sizes are also the largest. When considering the grain size dependence of fct phase formation, the inserted C layers suppress the fct phase formation by limiting grain growth. The mechanism of carbon additives in the disorder-order transformation of FePt/C thin films is not clear. One possibility is that the ordering process was

enhanced by defects included in the FePt grains after the C additive atoms intermixed into the FePt layers so that the ordering temperature could be lowered. However, for the thicker carbon layer films, it requires larger activation energy to break the carbon layers and to activate the intermixing process.

#### 3.3.6.4 Implantation effect

Implanted samples have similar coercivity and smaller grain size when compared with the un-implanted ones. From Table 3.3, the implanted sample, (e), has the largest (001)/(002) ratio. This means that it has the most complete fcc-fct phase transformation in its grains among the samples shown. The long range ordering provides the films with large coercivity despite of its small grain size. This implies that ions implantation may help to enhance the degree of long range ordering in individual grains, making it possible to make films to have large coercivity with smaller "high quality" grains.

## 3.4 Summary

The ~10 nm thick (3-cycle) and ~25 nm thick (9-cycle) FePtC multilayer films have been prepared and studied and their properties have been compared with Chiah's ~50 nm thick films. Although the grain size can be limited in thinner films, the coercivity is reduced. This means higher temperature treatment is needed for thinner films to be in ordered phase with sufficiently large coercivity. On the other hand, post-deposition carbon ions implantation is found to be able to increase the degree of long range order of the FePt grains.

## Reference

[1] M.F. Chiah, "Characterization of Magnetic Nanocomposite Thin Films for High Density Recording Prepared by Pulsed Filtered Vacuum Arc Deposition", Ph.D. thesis, The Chinese University of Hong Kong (2004)
[2] Y.K.Takahashi, T. Koyama, M. Ohnuma, T. Ohkubo, and K. Hono , J. Appl. Phys. **95**, 2690 (2004)
[3] Micheal F. Toney, Wen-Yaung Lee, J. A. Hedstrom, and A. Kellock, J. Appl. Phys. **93**, 9902 (2003)
[4] C.L.Platt K.W. Wierman, E.B. Svedberg, R. van de Veerdonk, and J.K. Howard, J. Appl. Phys. **92**, 6104 (2002)
[5] D. Ravelosona, C. Chappert and V. Mathet, Appl. Phys. Lett. **76**, 236 (2000)
[6] Quan Li, K.W. Kwong , Phys. Rev. Lett.. **92** 186102 (2004)

# Chapter 4

# *Characterization of FePt-Cu Nanocomposite Thin Film*

In this chapter, the preparation of FePt-Cu thin films with different total thickness, and different spacer thickness will be described. Then characterization of these films using RBS, XRD and VSM will be discussed.

## 4.1 Experiment design

In Chiah's work [1], it was shown that with the introduction of copper additive into the multilayer FePt films the ordering temperature could be lowered to 300°C. However, the grain size of the corresponding nanocomposite film is larger than 10 nm, which is too large for ultrahigh density recording media. Just like FePt-C samples discussed in the last chapter, restriction in the total film thickness has also been employed in the FePt-Cu films in order to limit the grain growth. FePt-Cu films with 25 nm and 10 nm thickness have been prepared and characterized.

## 4.2 Experiment detail

Again, multilayer structures have been employed in depositing all FePt-Cu films. Iron, platinum and copper were deposited separately on thermally grown $SiO_2$ films by the PFVAD system. By monitoring the charge counter of the PFVAD system, thickness of each element deposited can be precisely controlled. A - 80 V DC bias was applied

to the substrate. The iron, platinum and copper cathode sources were operated separately in pulse mode with a 2.5 ms pulse duration and a frequency of 4 pulses/s. No substrate heating is applied during deposition. Shown in Fig. 4.1 is a schematic diagram of the multilayer films.

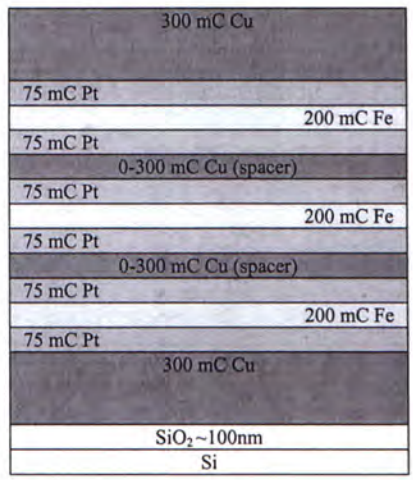


Fig. 4.1 Schematic of "3-cycle" multilayer FePtCu film

The multilayer Fe/Pt films are separated by several copper spacer layers of different thickness. Also, just like in the study of the FePt-C films, both 3-cycle and 9-cycle FePt-Cu films have been prepared to investigate the total film thickness dependence of the FePt fct phase formation.

Thermal annealing was performed at 370-570°C in argon atmosphere for 10 minutes after deposition.

## 4.3 Results and discussion

### 4.3.1 RBS measurements

In the PFVAD system, the thickness of the deposited film is monitored by the integrated charge arriving at the substrate. As a calibration, 1000 mC of Cu were deposited on $SiO_2$ and its thickness was determined by RBS measurement. Shown in Fig. 4.2 is the RBS spectrum of this film. The result is tabulated in Table 4.1.

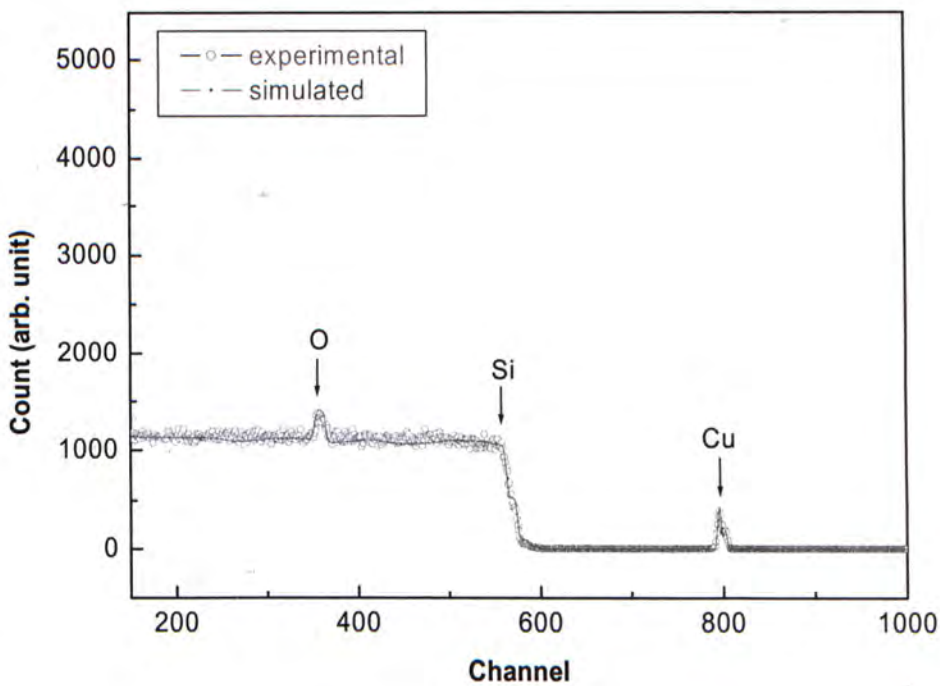


Fig. 4.2 RBS spectrum of 1000 mC Cu deposited on $SiO_2$

| | Charge counted (mC) | Thickness (nm) |
|---|---|---|
| Cu | 1000 | 3.5 |

Table 4.1 Fitted thickness of the 1000mC Cu from RBS spectrum

Based on the charge-to-thickness relationship found, multilayer films with different total thickness and composition were designed and deposited. Shown in Fig. 4.3 is the RBS spectrum of the as-deposited 3-cycle FePtCu multilayer film and the film structure model built from the deposition sequence. The experimental spectrum was fitted with the model and then the thickness of each layer was estimated. Shown in Fig. 4.4 is the RBS spectrum of the as-deposited 9-cycle FePtCu film with the corresponding film structure model. The fitted result is tabulated in Table 4.2.

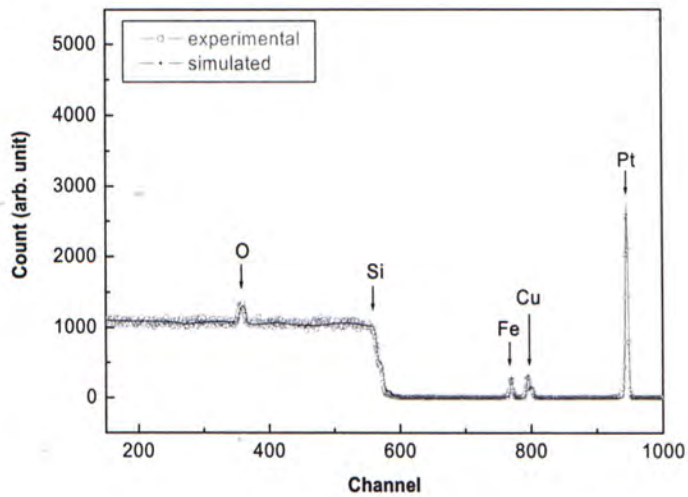


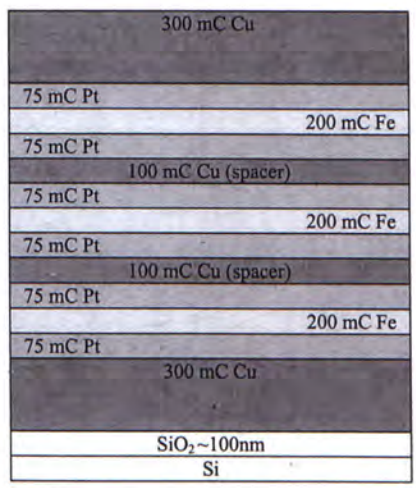


Fig. 4.3 (a) RBS spectrum of a 3-cycle FePtCu film with 100 mC Cu spacer layers and (b) multilayer film model used in fitting

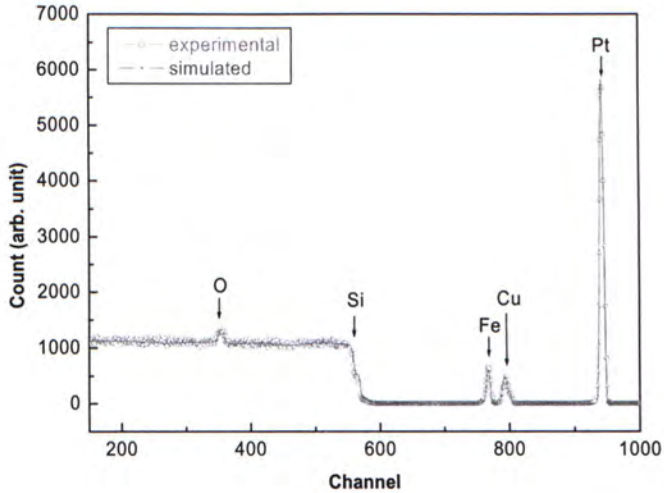


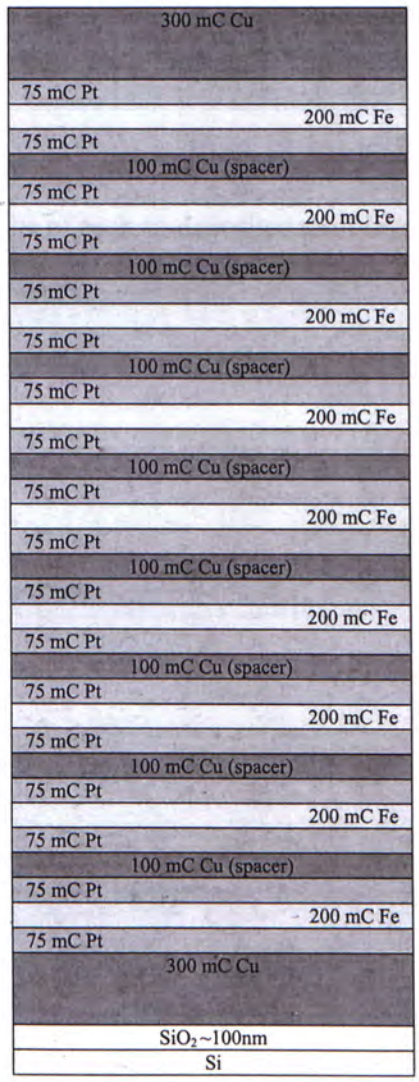


Fig. 4.4 (a) RBS spectrum of a 9-cycle FePtCu film with 100 mC Cu spacer layers and (b) multilayer film model used in fitting

| | Spacer deposited | Spacer (Cu) thickness | Pt thickness (75mC) | Fe thickness (200mC) | Elemental ratio | Total thickness |
|---|---|---|---|---|---|---|
| 3-cycle | 0mC | 0 | 0.5 | 0.9 | $Fe_{37}Pt_{30}Cu_{33}$ | 7.1 |
| | 100mC | 0.4 | 0.5 | 0.8 | $Fe_{31}Pt_{29}Cu_{40}$ | 7.7 |
| | 200mC | 0.8 | 0.5 | 0.8 | $Fe_{29}Pt_{25}Cu_{46}$ | 8.1 |
| 9-cycle | 0mC | 0 | 0.5 | 1.0 | $Fe_{50}Pt_{37}Cu_{13}$ | 19.9 |
| | 100mC | 0.4 | 0.5 | 0.8 | $Fe_{38}Pt_{34}Cu_{28}$ | 20.2 |
| | 200mC | 0.8 | 0.6 | 0.7 | $Fe_{27}Pt_{36}Cu_{37}$ | 23.8 |

Table 4.2 The fitted results of each as-deposited multilayer film from RBS spectra

### 4.3.2 XRD measurements

The structural properties of the films were studied by a glancing angle x-ray diffractometry with the incident angle of 1°. Shown in Fig. 4.5 are the XRD spectra of the 3-cycle FePtCu film annealed at 470°C with different values of copper spacer thickness, ranging from 0 to 0.8 nm. The result indicates that the transformation temperature strongly depends on the copper spacer thickness. In the film without a Cu spacer (0 nm), the fct peak is hardly visible, if any, and the main (111) peak is relatively broad. In the sample with a 0.4 nm thick Cu spacer, the fct (001) and fct (110) peaks are clearly observed indicating the disorder-order transformation has started. Moreover, the main (111) peak becomes sharper than that of the previous sample without a Cu spacer. This means the grain growth in the sample with a Cu spacer is faster. The intensity of the fct peaks however becomes weaker when the Cu spacer thickness increases to 0.8 nm.

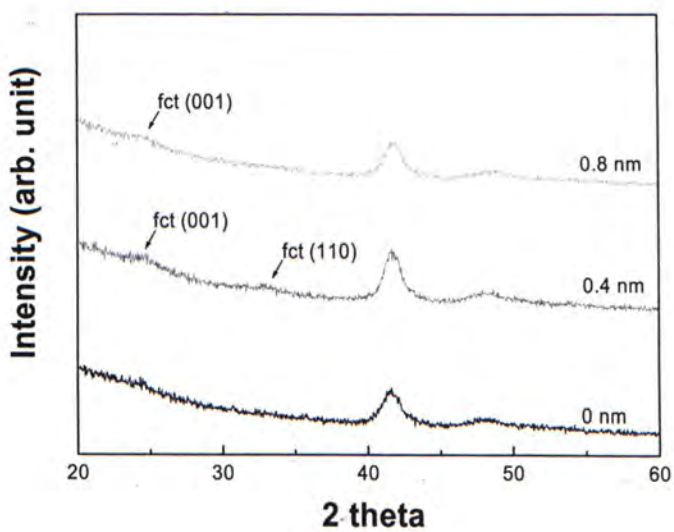


Fig. 4.5 XRD spectra of the 3-cycles FePtCu films annealed at 470°C with different copper spacer thickness

Shown in Fig. 4.6 is a plot of the grain sizes of these samples against Cu spacer thickness. The grain sizes were estimated by Scherrer's formula using the (111) peak FWHM. This plot shows that the sample with a 0.4 nm thick Cu spacer has the largest grain size. When compared with the plot of grain size of FePtC samples shown in Fig. 3.8, they show different trend. In the FePtC samples, the film without a spacer has the largest grains and the grain size decreases with increasing spacer thickness. However in the FePtCu samples, the films with a Cu spacer have larger grains than that without a spacer. It seems that with the inserted Cu spacers, there is grain growth enhancement.

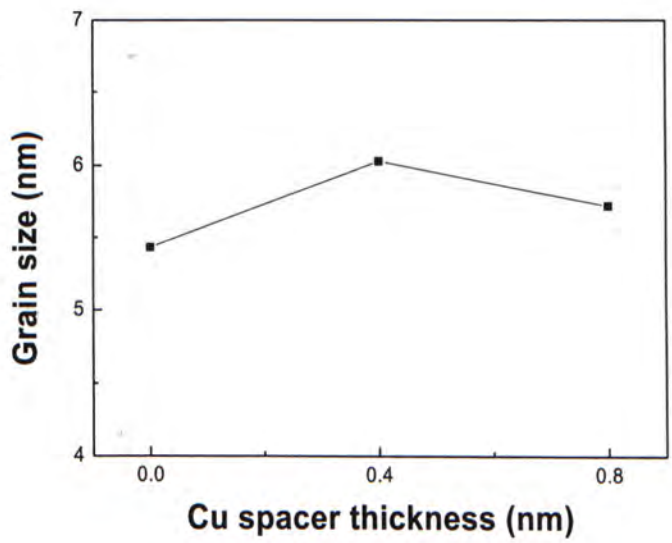


Fig. 4.6 Grain size of 3-cycle FePtCu samples with different copper spacer thickness annealed at 470°C

### 4.3.3 VSM measurements

The magnetic properties were studied by vibrating sample magnetometery. Magnetic hysteresis loops were obtained at 300K in the presence of an in-plane applied field. Shown in Fig. 4.7 are the hysteresis loops of the 3-cycle FePtCu films annealed at 570°C with different Cu spacer thickness, ranging from 0 to 0.8 nm. The sample with a 0.4 nm thick Cu spacer shows the largest coercivity indicating the disorder-order transformation in this sample is more complete. The magnetic result agrees with the XRD result which also showed that the fct peaks are more significant in this sample. The fcc-fct phase transformation is enhanced by inserting thin layers of Cu between the FePt layers. But when the spacer layers become thicker, the enhancement effect however reduces. This may be an indication that the disorder-order transformation enhancement mechanisms of C and Cu in FePt are different. A more detailed discussion will be presented in the following section.

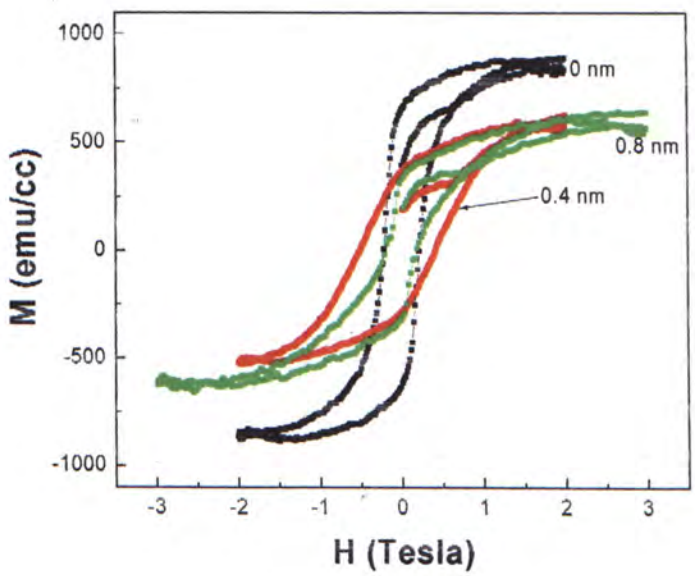


Fig. 4.7 Hysteresis loops of 3-cycles FePtCu annealed at 570°C with different copper spacer thickness

Shown in Fig. 4.8 is the plot of coercivities of 3-cycle and 9-cycle FePtCu samples with different Cu spacer thickness and annealing temperatures. Hollow circles represent the 3-cycle samples and the solid circles represent the 9-cycle samples. The same colour is used for the samples with the same annealing temperature. In the 2 red curves, they both show that all FePtCu samples have small coercivities after annealing at 370°C. The values of the coercivity are about the same as the as-deposited samples (not shown). This means that the disorder-order transformation has not started in such a low annealing temperature in the FePtCu samples. When the annealing temperature is increased to 470°C and 570°C, corresponding to the blue and green curves respectively, the coercivities increase accordingly. When comparing both pairs of curves, the 9-cycle samples have larger coercivities that the 3-cycle samples with the same Cu spacer thickness. This agrees with the findings in the FePtC samples and suggests that there is grain size dependence in the fcc-fct transformation. On the other hand, all curves show a peak at the 0.4 nm Cu spacer thickness. This suggests that Cu has a different role as C in FePt phase formation. There is an optimal Cu spacer thickness to achieve a more complete fcc-fct phase transformation in FePt film. This finding is in agreement with the results of Chiah [1] and will be discussed in the following section.

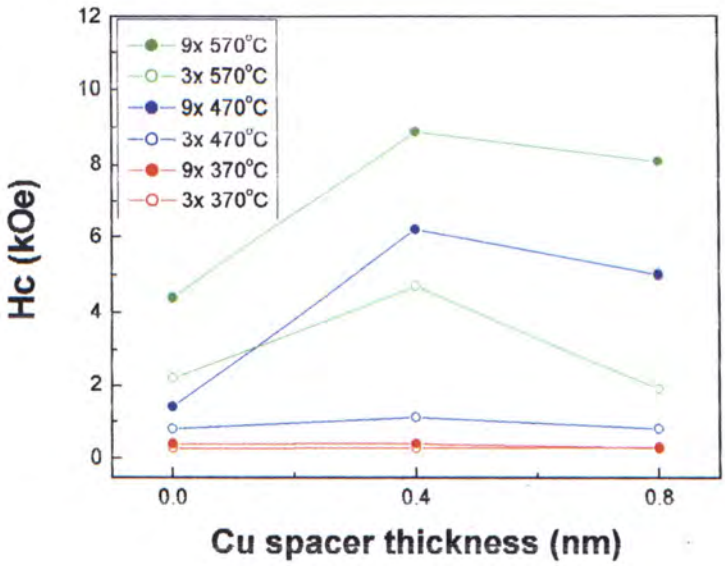


Fig. 4.8 Coercivity of 3-cycle and 9-cycle FePtCu samples with different copper spacer thickness annealed at various temperature for 10 minutes

### 4.3.4 Discussion

#### 4.3.4.1 Total film thickness

Shown in Fig. 4.9 is the plot of the coercivities of the FePtCu samples annealed at different temperatures including Chiah's results for his 50 nm FePtCu samples. At 370°C, Chiah's sample has a coercivity larger than 5 kOe, while the coercivities of the 3-cycle and 9-cycle samples are much smaller than 0.5 kOe. As the annealing temperature increases, the coercivities of both the 3-cycle and 9-cycle samples increase. However, the coercivities of the 9-cycle samples are always larger than those of the 3-cycle samples. This shows the same trend as in the FePtC samples which can be explained by grain size dependence of the phase transformation. Thicker films have more nucleation sites for grain growth and is therefore also in favor of the fcc-fct phase transformation.

In both the FePtC and FePtCu films, the film coercivity greatly depends on the total film thickness: the thinner the film, the smaller is the coercivity. In other words, the thinner the film, the higher is the ordering temperature. This implies that if we want to limit the grain growth by limiting the vertical dimension, there will be a trade-off in the increase of the ordering temperature.

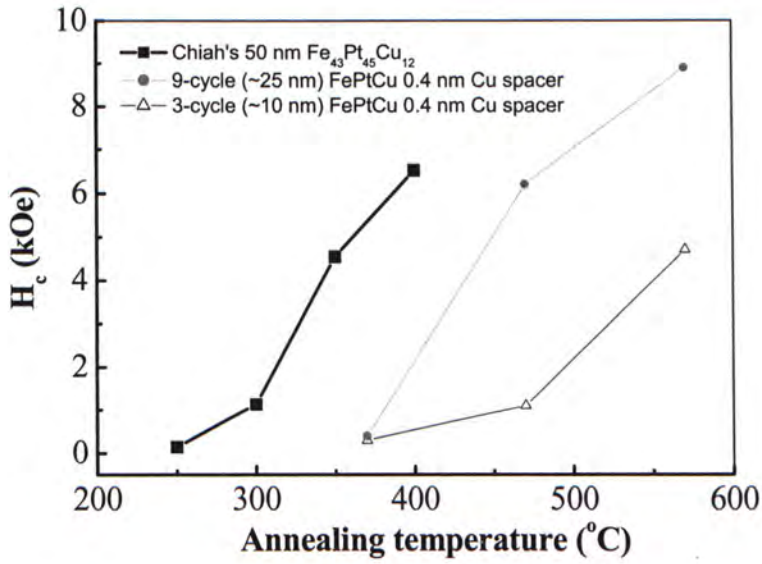


Fig. 4.9 Coercivities of FePtCu samples annealed at different temperature

#### 4.3.4.2 Cu spacer thickness

In the FePtC samples, film coercivities decrease with increasing C spacer thickness. However in the samples with Cu as additive, the samples without a Cu spacer have relatively small coercivities. The coercivities increase to a maximum in samples with a thin Cu spacer. Then they decrease again in samples with a thicker Cu spacer. This provides evidence that the mechanisms in enhancing the fcc-fct phase transformation by adding C and Cu are different. The C atoms have low solubility in both Fe and Pt. They tend to diffuse out of the FePt lattice after annealing at progressively higher temperatures, and hence lead to lattice vacancies and defects, through which enhancement of the order-disorder transformation of FePt is achieved. On the other hand, it has been suggested that Cu can form a stable alloy with FePt which can enhance the phase transformation [2-3]. As Cu has a similar atomic volume as that of Fe, the diffusion length of Cu atoms inside the film is limited. Therefore, the Cu atoms in the top and bottom layers are not able to diffuse deep into the middle of the

film nor to form alloy with the FePt layer in the middle of the film. The inserted Cu spacer layers can however provide extra Cu atoms to form FePtCu alloy inside the film thus enhancing the phase transformation. But in the case of thicker spacer samples, the Cu spacer layers are too thick that merging of grains across layers are prevented. Therefore small grains remain in different layers. The small grain size does not favor fcc-fct transformation hence leading to smaller coercivities.

On the other hand, it is noted that in the samples without a Cu spacer, the coercivities are so small that they are even smaller than those of pure FePt films! This means that the top and bottom Cu layers somehow suppress the fcc-fct phase transformation. To verify this statement, FePtCu samples without the top and bottom Cu layers were prepared. Shown in Fig. 4.10 are the hysteresis loops of the 3-cycle FePtCu samples (with 0.4 nm Cu spacer layers) with and without Cu top and bottom layers. The samples were annealed at 470°C for 10 minutes. The one without the top and bottom Cu layers shows a larger coercivity. Similar experiments were performed for the 9-cycle samples and similar results were obtained as shown in Fig. 4.11. The shoulder-like shape in the hysteresis of the sample without Cu top and bottom layers indicates that there are two decoupled phases, the hard fct phase and the soft fcc phase, in the film. While there are some recent reports on the suppression of the fcc-fct phase transformation by adding Cu into the films [4, 5], there are also published works showing that Cu is able to accelerate the fct phase formation [2, 3]. Further investigation is needed to find out the exact role of Cu in the FePt system.

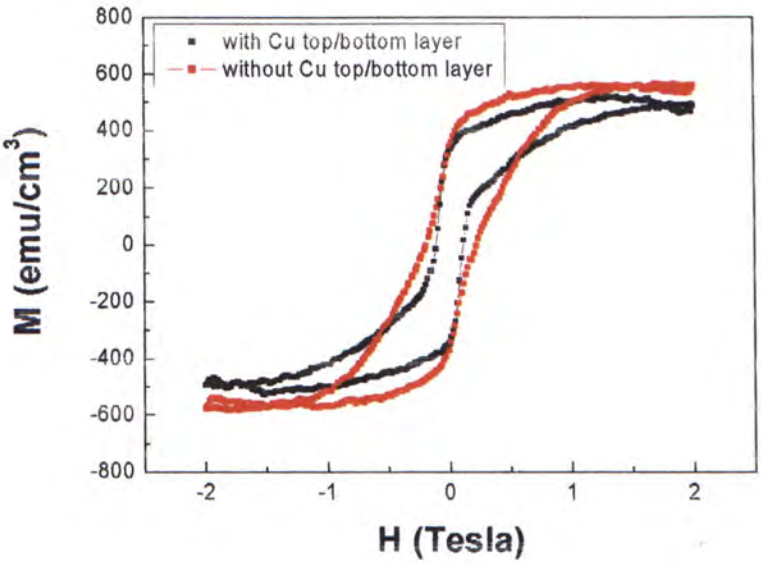


Fig. 4.10 Hysteresis loops of 3-cycle FePtCu samples (with 0.4 nm Cu spacer layers) with and without Cu top and bottom layers after annealing at 470°C for 10 minutes.

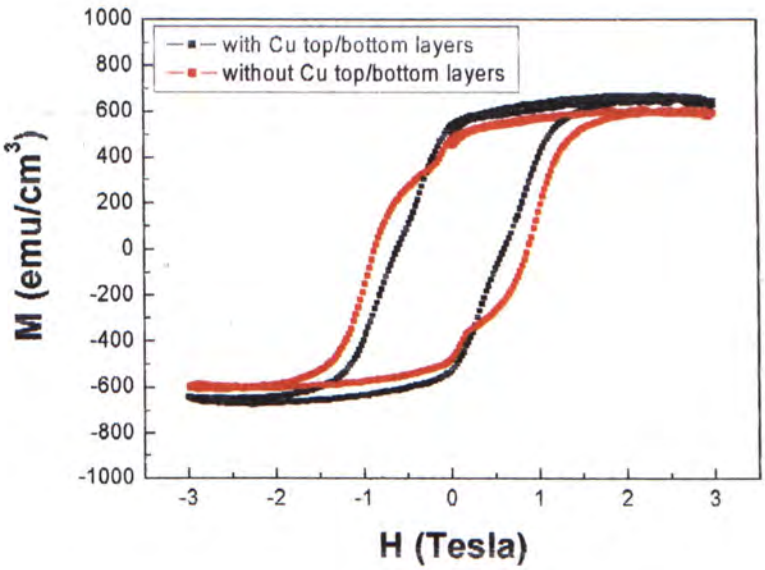


Fig. 4.11 Hysteresis loops of 9-cycle FePtCu samples (with 0.4 nm Cu spacer layers) with and without Cu top and bottom layers after annealing at 470°C for 10 minutes.

### 4.4 FePt films without additive

For comparison, 3-cycle and 9-cycle multilayer FePt films without additive atoms have been prepared by PFVAD. Shown in Fig. 4.12 is the XRD spectra of the two films annealed at 470°C. Obviously, the 9-cycle sample show more significant fct peaks which means the fcc-fct transformation is more complete than the 3-cycle one at the same annealing temperature. Grain size is estimated by Scherrer's formula using the FWHM of the (111) peak and is tabulated in Table 4.3. Their grain sizes are larger than those of the FePtC and FePtCu films with similar thickness and annealing conditions. This implies that without the limiting effects on grain growth due to the additive atoms, large grains can be formed by merging of small FePt grains from all layers. Shown in Fig. 4.13 are the hysteresis loops of the two samples without additive atoms annealed at 470°C. The coercivity of the 9-cycle sample is larger than that of the 3-cycle sample. This supports the observation in the XRD spectra that the 9-cycle sample has gone through a more complete phase transformation hence a larger coercivity is obtained.

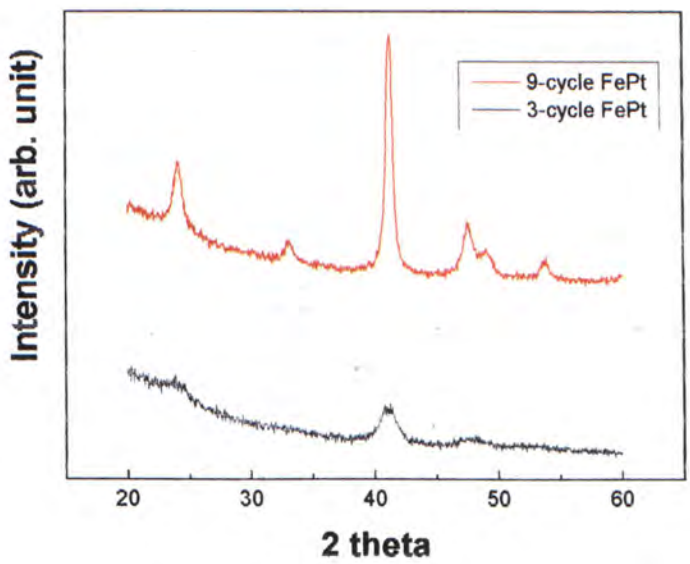


Fig. 4.12 XRD spectra of 3-cycle and 9-cycle FePt films annealed at 470°C.

| | Grain size after annealing at 470°C |
|---|---|
| 3-cycle FePt | 6.3 nm |
| 9-cycle FePt | 12.1 nm |

Table 4.3 Grain size of pure FePt multilayer film

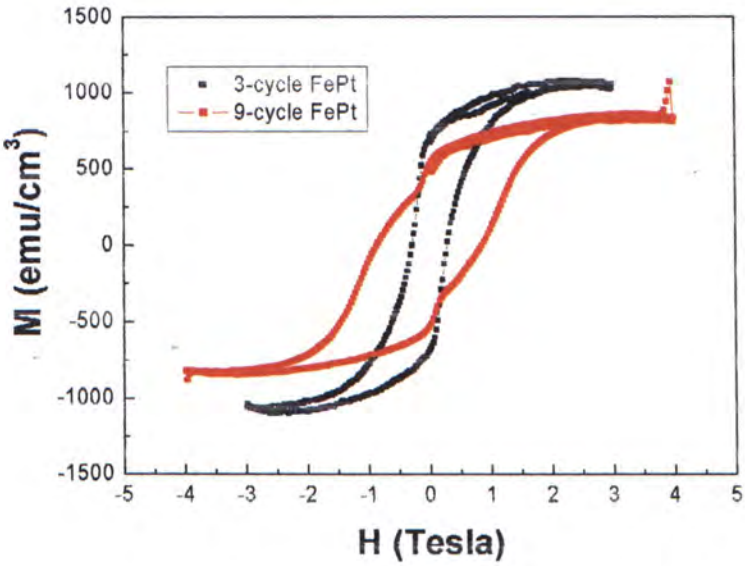


Fig. 4.13 Hysteresis loops of 3-cycle and 9-cycle FePt films annealed at 470°C.

## 4.5 Summary

The ~10 nm thick (3-cycle) and ~25 nm thick (9-cycle) FePtCu multilayer films have been prepared and studied and their properties have been compared with those of Chiah's ~50 nm thick films. Similar to the FePtC samples, the thinner films are found to have smaller coercivities. The phase formation enhancement mechanism of Cu in FePt is believed to be different with that of C. On the other hand, it was found that the top and bottom Cu layers suppress the fcc-fct phase transformation. The reason for such a phenomenon is not clear at the moment and needs further investigation to find out the exact role of Cu as an additive in the FePt system.

**Reference**

[1] M.F. Chiah, "Characterization of Magnetic Nanocomposite Thin Films for High Density Recording Prepared by Pulsed Filtered Vacuum Arc Deposition", Ph.D. thesis, The Chinese University of Hong Kong (2004)

[2] T. Maeda, A. Kikitsu, T. Kai, T. Nagase, H. Aikawa, and J. Akiyama, IEEE Trans. Magn. **38**, 2796 (2002)

[3] C.L. Platt, J. Appl. Phys. **95**, 609 (2002)

[4] K.W. Wierman, C.L. Platt, J.K. Howard, J. Magn. Magn Mater. **278**, 214-27 (2004)

[5] X. Sun, S. Kang, J.W. Harrell, and David E. Nikles, J. Appl. Phys. **93**, 7337 (2003)

# *Chapter 5*

# *Conclusion and Future Works*

## 5.1 Conclusion

Materials with high uniaxial magnetocrystalline anisotropy such as FePt in $L1_0$ (fct) phase, are attractive for ultra-high-density magnetic recording applications because they could provide smaller magnetic grains while maintaining a sufficiently high thermal stability. Normally, post-annealing at temperatures higher than 600°C is needed to achieve the $L1_0$ phase. The high temperature process is not desirable for the industry. Great effort has been put to lower the ordering temperature of the desired phase. Chiah [1] has investigated the influence of C and Cu additives on the $L1_0$ ordering and grain growth of the multilayer-deposited FePt films. However, the grain sizes of the ordered films are too large for application.

In this project, thinner FePt-C and FePt-Cu multilayer films were prepared by filtered vacuum arc deposition. The reduction in film thickness was expected to be able to limit grain growth during annealing. Also, post deposition carbon ion-implantation was performed for some samples aiming at enhancing the ordering transformation of the FePt grains.

Our results show that the degree of the fct phase ordering generally decreases with decreasing film thickness. Besides ordering, grain size is also reduced in thinner film. This supports the argument that the disorder-order transformation is grain size dependent. Since there is less amount of FePt and also the restriction in dimension for the grain growth in thinner films, small grain size will result. However, while the goal

of limiting grain size is achieved in thinner film, the degree of ordering is also reduced. Hence higher annealing temperature is required to achieve the same coercivity as in thicker film.

The implanted FePtC samples were found to have similar coercivity and smaller grain size when compared with the un-implanted one. Their relatively large (001)/(002) ratio in XRD spectra explains why they have such large coercivity despite of the small grain size. It is believed that the ion bombardment process has led to atomic displacements that favour local atomic arrangements and lattice relaxation, hence leading to enhancements in the phase formation during annealing [2]. Our preliminary results suggest that the ion implantation process is helpful to enhance the degree of long range ordering in individual grains, and it is a promising method to produce films with a large coercivity while maintaining sufficiently small "high quality" grains.

It is shown that the chemical ordering of FePt greatly depends on the additive spacer thickness. The degree of the fcc-fct phase transformation simply decreases with increasing spacer thickness in the FePt-C samples. The C atoms have low solubility in both Fe and Pt. They tend to diffuse out of the FePt lattice after annealing at progressively higher temperatures, and hence lead to lattice vacancies and defects, through which enhancement of the order-disorder transformation of FePt is achieved. In FePtCu films, the chemical order reaches a maximum when thin Cu spacer layers are inserted between the FePt layers. This indicates that the phase transformation enhancement mechanisms are different of the two additives. However, it requires further investigation to understand the exact role of the Cu additives in the FePt system.

## 5.2 Future works

Perpendicular recording has been demonstrated in research laboratories recently [3]. The superparamagnetic limit can then be pushed further. Nevertheless, the limit will come sooner or later. High magnetic anisotropic material is believed to be the promising solution and research work in this field is still actively on going. In this work, it is found that reducing the film thickness can limit grain growth but at the same time will lead to a lower coercivity, or a higher ordering temperature. Nevertheless, ion-implantation seems to be able to increase the chemical ordering of individual grains such that a smaller grain can provide a relatively large coercivity. By making use of the advantage of the pulsed filtered vacuum arc deposition system, ion implantation can be done at various dose and energies right after the multilayer film deposition. As the sample implanted by 8 keV C has larger coercivity than the un-implanted one, we can implant different C dose while keeping the substrate bias at 8 kV to investigate the dose effect. Moreover, the deposition and implantation sequence can be interchanged easily so that an implantation process can be performed right after the deposition of a layer of FePt, and the sequence can be repeated or changed in a very flexible manner. It seems that the combination of the multilayer deposition and ion implantation processing approach could provide a lot of new possibilities in tuning the structural and magnetic properties of these magnetic nanocomposite thin films to suit the future application needs and is worth further investigations.

**Reference**

[1] M.F.Chiah, "Characterization of Magnetic Nanocomposite Thin Films for High Density Recording Prepared by Pulsed Filtered Vacuum Arc Deposition", CUHK thesis (2004)

[2] D. Ravelosona, C. Chappert, et al., Appl. Phys. Lett. 76, 236 (2000)

[3] http://www.hitachigst.com

# *Appendix 1*

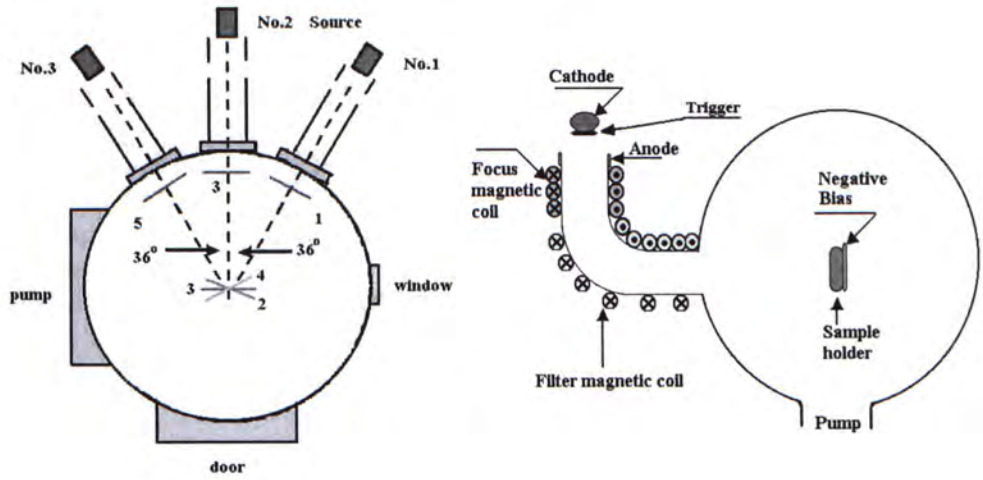


Fig. 2.1 Schematic of the PFVAD system; (a) top-view; (b) side-view.

Pressure during deposition: $<4x10^{-4}$Pa

| | Pt | Fe | C | Cu |
|---|---|---|---|---|
| Bias | 100 V | 100 V | 100 V | 100 V |
| Focus | 120 uA | 120 uA | 80 uA | 80 uA |
| Arc | 120 V | 120 V | 100 V | 100 V |
| Trigger | 150 V | 150 V | 150 V | 150 V |
| Deflect | 160 uA | 160 uA | 150 uA | 150 uA |

Bias: Applied between the anode and the filter duct. It s used to restain the ions in the plasma arriving at the duct.

Focus: Provides current for the focus solenoid to generate magnetic field, which focuses the plasma from the source.

Arc: Applied between the cathode and anode electrodes to pulsely sustain the main arc.

Trigger: It is applied between the trigger and the cathode electrodes. When a pulsed high voltage applied between trigger and cathode, there is a spark produced which initiates the arc.

Deflect: It is applied on the guiding solenoid to produce filtering and guiding magnetic field for the plasma.

# *Appendix 2*

Shown in Fig. A.1 are the RBS spectra of a 9-cycle FePtC sample with simulated curves of fitting models with different Fe thickness. The graphs show that the experimental curve is best fitted with simulated curve of 0.9 nm Fe thickness. Both the 1.0 nm and 0.8 nm Fe simulated curves don't fit the experimental curve well. This indicates that the accuracy of the fitting is 0.05 nm.

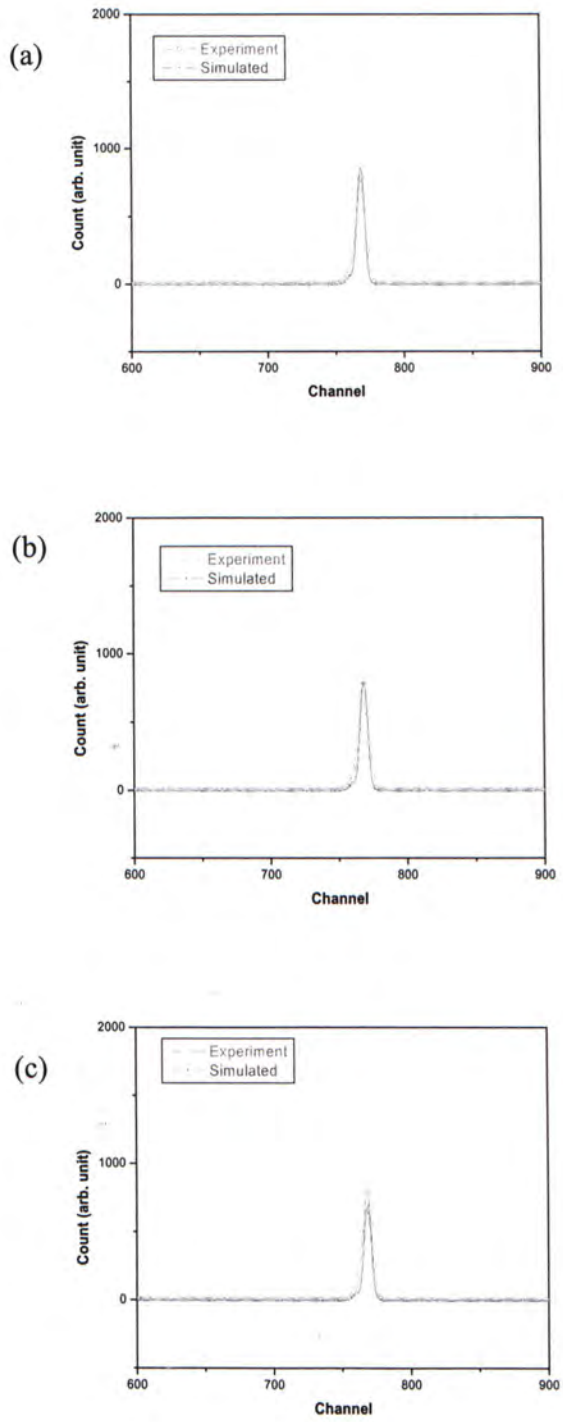


Fig. A.1 RBS spectra of 9-cycle FePtC with simulated curves of fitting models with (a) 1.0 nm Fe, (b) 0.9 nm Fe and (c) 0.8 nm Fe